

What would dense atmospheric observation networks bring to the quantification of city CO₂ emissions?

Lin Wu¹, Grégoire Broquet¹, Philippe Ciais¹, Valentin Bellassen^{2,*}, Felix Vogel¹, Frédéric Chevallier¹, Irène Xueref-Remy¹ and Yilong Wang¹

[1] Laboratoire des Sciences du Climat et de l'Environnement (LSCE), UMR CEA-CNRS-UVSQ, Gif sur Yvette, France

[2] CDC Climat, 75009 Paris, France

[*] Now at INRA, UMR 1041 CESAER, 21000 Dijon, France

Correspondence to: L. Wu (lwu@lsce.ipsl.fr)

Abstract

Cities, currently covering only a very small portion (<3%) of the world's land surface, directly release to the atmosphere about 44% of global energy-related CO₂, but are associated with 71-76% of CO₂ emissions from global final energy use. Although many cities have set voluntary climate plans, their CO₂ emissions are not evaluated by the Monitoring, Reporting and Verification (MRV) procedures that play a key role for market- or policy-based mitigation actions. Here we analyse the potential of a monitoring tool that could support the development of such procedures at the city scale. It is based on an atmospheric inversion method that exploits inventory data and continuous atmospheric CO₂ concentration measurements from a network of stations within and around cities to estimate city CO₂ emissions. This monitoring tool is configured for the quantification of the total and sectoral CO₂ emissions in the Paris metropolitan area (~12 million inhabitants and 11.4 TgC emitted in 2010) during the month of January 2011. Its performances are evaluated in terms of uncertainty reduction based on Observing System Simulation Experiments (OSSEs). They are analyzed as a function of the number of

sampling sites (measuring at 25 meters above ground level) and as a function of the network design. The instruments presently used to measure CO₂ concentrations at research stations are expensive (typically ~50 k€ per sensor), which has limited the few current pilot city networks to around ten sites. Larger theoretical networks are studied here to assess the potential benefit of hypothetical operational lower-cost sensors. The setup of our inversion system is based on a number of diagnostics and assumptions from previous city scale inversion experiences with real data. We find that, given our assumptions underlying the configuration of the OSSEs, with 10 stations only, the uncertainty for the total city CO₂ emission during one month is significantly reduced by the inversion, by ~42%. It can be further reduced by extending the network, e.g. from 10 to 70 stations, which is promising for MRV applications. With 70 stations, the uncertainties in the inverted emissions are reduced significantly over those obtained using 10 stations by 32% for commercial and residential buildings, by 33% for road transport, by 18% for the production of energy by power plants, and by 31% for total emissions. These results indicate that such a high number of stations would be likely required for the monitoring of sectoral emissions. They demonstrate some high potential that atmospheric inversions can contribute to the monitoring and/or the verification of city CO₂ emissions (baseline) and CO₂ emission reductions (commitments) and the advantage that could be brought by the current developments of lower-cost medium precision (LCMP) sensors.

1 Introduction

At the 2010 Cancun summit, parties from the United Nations Framework Convention on Climate Change (UNFCCC) agreed to set up a target of keeping global warming under 2°C compared to pre-industrial levels (UNFCCC, 2011; Meinshausen et al., 2009; Ciais et al., 2013). Shah et al. (2013) showed that this 2°C global warming target is economically and technically feasible, albeit demanding a mitigation of the Greenhouse Gases (GHG) emissions across all sectors of anthropogenic activities. Many developed and developing countries consequently have made commitments to reduce their emissions under the UNFCCC. National commitments focus on the land use sector or on economy-wide activities such as electricity production and industrial processes. There is however a gap between these commitments and the requirements on the emission reductions (often referred to as “emission gap”) for achieving the 2°C global warming target (UNEP, 2013).

1 Cities occupy less than 3% of the world's land surface (Liu et al., 2014), but directly release
2 about 44% of the global energy-related CO₂ and are responsible for 71-76% of CO₂ emissions
3 from global final energy use (Seto et al., 2014). This urban share of the anthropogenic
4 emissions will continue to increase in the context of an accelerating urbanization process
5 (IEA, 2008). The global urban population has grown from 746 million in 1950 to 3.9 billion
6 in 2014, and it is expected to grow by 2.5 billion people by 2050, with nearly 90% of them
7 living in Asia and Africa (UN, 2014).

8 City mitigation options, such as the improvement of public transportation infrastructures
9 using Mass and Rapid Transit (MRT) systems, of building retrofits, and of energy/waste
10 recycling, and the development of district heating/cooling plants (Sugar and Kennedy, 2013;
11 Erickson and Tempest, 2014), can significantly contribute to bridging the emission gap. This
12 plausible additional city contribution could cover ~15% of the total emission reduction
13 required to reach the 2°C global warming target, and represents up to two-thirds of the level
14 of emission reduction covered by the national commitments (Erickson and Tempest, 2014).
15 Large urban areas have a strong potential to decrease per capita CO₂ emissions for some
16 important sectors (e.g. transportation and heating) where clusters of population and economic
17 activities can share common infrastructures (Bettencourt et al., 2007; Dodman, 2009; Glaeser
18 and Kahn, 2010; CDP, 2012).

19 Thousands of cities declared to be willing to take actions to report and reduce their CO₂
20 emissions (Rosenzweig et al., 2010; Reckien et al., 2013). Such efforts can decrease their
21 climate vulnerability and foster co-benefits in terms of air quality, energy access, public
22 health, and city livability (Seto et al., 2014). They may also foster significant local economic
23 development through advances in green technology. For instance, the London low carbon
24 environmental goods and services sector is estimated to have generated more than £25 billion
25 revenue for 2011/12 (BIS, 2013).

26 To check whether claimed reduction targets are fulfilled, the present-day city emissions have
27 to be known accurately to define a baseline upon which reductions are defined, and these
28 emissions will have to be monitored over time during the agreed-upon reduction period. Such
29 quantification of emissions and emission reduction echoes the concept of Monitoring,
30 Reporting, and Verification (MRV) that is the cornerstone of most market- or policy-based
31 mechanisms in climate economy (Bellassen and Stephan, 2015). It ensures that the mitigation
32 actions are properly monitored and reported, and that the mitigation outcomes can be verified.

1 The MRV has been widely applied in many contexts such as projects, organizations, policies,
2 sectors, or activities within territories (see Bellassen and Stephan (2015) and references
3 therein). For diverse applications, MRV can rely upon different standards, but requires
4 transparency, quality, and comparability of information about emission accounting and the
5 mitigation action implementations.

6 The first urban mitigation actions relevant for MRV are those whose impacts are relatively
7 easy to measure, e.g., projects and Programmes of Activities (PoA) under the Clean
8 Development Mechanism (CDM) as well as efforts on emission reductions for large factories
9 and buildings under the Tokyo Emission Trading Scheme (ETS) (Clapp et al., 2010; IGES,
10 2012; Marr and Wehner, 2012; UNEP, 2014). However, there is a lack of technical capacity
11 for accurate accounting of diffuse sources, e.g. transportation and residential buildings. This
12 lack of capacity makes MRVs for citywide emissions challenging (Wang-Helmreich et al.,
13 2012; UNEP, 2014), and may hinder citywide mitigation implementation in the absence of
14 strong political will, sufficient institutional governance and financial support. Hitherto MRV
15 practices for urban mitigation actions are still limited and the majority of sources within the
16 city territory remain uncovered. For instance, the Tokyo ETS – the most advanced urban ETS
17 scheme – only regulates less than 20% of the city total emissions (TMG, 2010). In this
18 context, there is a keen need to scale up policy instruments and market mechanisms to better
19 support citywide mitigation actions (World Bank, 2010; Wang-Helmreich et al., 2012; The
20 Gold Standard, 2014). This gap may be reduced by new mechanisms such as the Nationally
21 Appropriate Mitigation Actions (NAMAs; recent move to raise pre-2020 emission reduction
22 ambitions by increasing access to climate financing) and the New Market-based Mechanism
23 (NMM; currently in negotiation for post-2020 carbon financing about crediting and trading of
24 mitigation outcomes). Both mechanisms are designed under UNFCCC to increase the
25 flexibility of mitigation actions so that broader segments of economy or policy-making can be
26 included in developed and developing countries (Howard, 2014; UNEP, 2014). Based on
27 estimates of emissions from the major sectors, a conceivable approach would be to set up
28 overall city mitigation targets and then negotiate specific targets for individual sectors or
29 groups of sources. Empowered by city-scale MRV (see UNEP (2014) for current
30 developments), city mitigation implementation could be (1) credited or traded under designed
31 mechanisms, and (2) registered for receiving international aid through climate finance.
32 However, ultimately, all these provisions for citywide mitigation actions and their MRV
33 necessitate the availability of accurate emission accounting methods.

1 The emission accounting methods that are usually suggested are inventories based on
2 statistical data (World Bank, 2010; Wang-Helmreich et al., 2012). Developing city-scale
3 inventories, and updating them over time, involves extensive collection of consistent and
4 comparable emissions data, which measures the level of activities (e.g. energy use statistics,
5 or in a more sector-specific manner, kilometers driven by vehicles, and volume of waste
6 provided to landfill) and the activity-to-carbon conversion rates (i.e. emission factor). In the
7 past, cities have followed diverse guidelines or protocols for emission inventory compilation,
8 and recently there is a trend of centralization e.g. with the newly proposed Global Protocol for
9 Community-Scale Greenhouse Gas Emission Inventories (GPC; Fong et al., (2014)) and the
10 UNFCCC reporting platform NAZCA (climateaction.unfccc.int). Admittedly, inventories of
11 city emissions are known to suffer from incomplete and uncertain data (see Appendix A for a
12 brief review of city inventories). For instance, there is usually a lack of precise statistics
13 regarding the total amount of fossil fuel that has been consumed within the cities. This
14 limitation impedes the practical use of city inventories in climate economy.

15 An improved emission accounting could rely on continuous atmospheric measurements of
16 CO₂ concentrations by networks of stations around and within cities. Indeed, accurate
17 measurement of the atmospheric signals, e.g. the CO₂ concentration gradients, provides
18 information about the emissions that is independent from the inventories. The statistical
19 method known as atmospheric inversion, which has been used for decades for improving the
20 knowledge of global and continental scale natural CO₂ fluxes (Enting, 2002; Bousquet et al.,
21 2000; Gurney et al., 2002; Peters et al., 2007; Chevallier et al., 2010; Broquet et al., 2013),
22 can be used to exploit atmospheric measurements for quantifying CO₂ emissions at the city
23 scale (McKain et al., 2012; Kort et al., 2013; Lauvaux et al., 2013; Hutyra et al., 2014; Bréon
24 et al., 2015). The principle of an inversion is to combine information from inventory data with
25 atmospheric CO₂ measurements to deliver improved emission estimates, i.e. estimates with a
26 reduced uncertainty, compared to the prior inventory. An inversion generally uses a 3D model
27 of atmospheric transport to relate emissions to observations. In just a few years, a number of
28 city atmospheric CO₂ measurement networks have been deployed for pilot studies. Examples
29 of cities where such networks have been deployed are Toronto (with 3 sites), Paris (with 5
30 sites), Recife (with 2 sites), Sao-Paulo (with 2 sites), Salt Lake City (~7 sites), Los Angeles
31 (~10 sites), and Indianapolis (with 12 sites). This creates a need to better document the
32 theoretical potential of atmospheric inversions to monitor emissions and their changes or to
33 independently verify inventories, with a quality relevant for city MRV applications. Urban

emissions are mainly connected to emissions from fossil fuel combustion, as other sources of urban emissions such as biofuel uses are usually very limited. Hence, for simplicity, we assume that urban emissions are all from fossil fuel combustion in our study.

Bréon et al. (2015), hereafter referred to as B15, used CO₂ measurements from 3 stations in the Paris area and a Bayesian inversion methodology to estimate CO₂ fossil fuel emissions in the Paris metropolitan area (the Île-de-France – IDF – region, which has ~12 million inhabitants) in winter 2010. The most resolved regional bottom-up inventory estimates that this area emitted 11.4 TgC in 2010 (AIRPARIF, 2013), an amount equivalent to ~12% of the CO₂ fossil fuel emissions from the whole France (Boden et al., 2013). B15 did not attempt to estimate sectoral emissions separately due to the very limited size of the measurement network they used. They rather focused on quantifying total CO₂ emissions from the Paris urban area. Staufer et al. (2016) refined the configuration of the inversion system of B15 and applied it for a one-year inversion of the Paris emissions.

In this paper, we assess the performance of atmospheric inversion for the monitoring of total and sectoral fossil fuel emissions in the Paris metropolitan area when using denser networks, based on Observing System Simulation Experiments (OSSEs). The objective is to analyze the sensitivity of this performance to the size and design (i.e. the location of the stations) of such networks, and thus to derive requirements on the configuration of the atmospheric inversion to provide different levels of accuracy on the estimates of the total and sectoral city emissions. We base our inversion methodology and the configuration of the OSSEs – notably the assimilation of concentration gradients and the practical configuration of the inversion parameters – on the system, expertise and diagnostics documented in B15 and Staufer et al. (2016). The use of much larger measurement networks still necessitates some assumptions regarding the inversion framework and the characterization of the sources of errors.

The CO₂ measurement instruments presently used for atmospheric inversion in the scientific community are rather expensive (typically ~50 k€ per sensor) which explains the limited size of the existing city networks. To bridge this data gap, national and European innovation projects (e.g. <http://www.climate-kic-centre-hessen.org/miriade.html>, MIRIADE-ANR: ANR-11-ECOT-0004) have been proposed to test lower cost (typically ~1 k€ per unit) sensors (called hereafter low-cost medium precision – LCMP – sensors) and to develop a corresponding calibration strategy which would enable the measurement of CO₂ concentrations with a precision and an accuracy that would be acceptable for city scale

inversions (but maybe not for other scales, for which more expensive instruments may still be needed for the foreseeable future). This motivates our tests, in this study, of networks with up to 70 sensors.

The principle of the inversion performance assessment, the inversion methodology and the OSSE setup are described in Sect. 2. The inversion results are analyzed in Sect. 3. Based on these results, Sect. 4 discusses requirements on the configuration of the observation network for achieving different targets of accuracy in the estimates of total and sectoral CO₂ emissions from the Paris area. Conclusions are drawn in Sect. 4.

2 Methodology

The principle and the configuration of our atmospheric inversion system are close to those of B15. The general principle is to estimate the emission budgets for different sectors of anthropogenic activity, areas and time windows, which all together constitute the total emissions of IDF for the month of January 2011. It corrects a prior estimate of these emission budgets given by an inventory to better fit observed concentration gradients between pairs of sites along the wind direction, in and around the Paris area, since such gradients characterize the enhancement of atmospheric CO₂ due to the Paris emissions. An atmospheric transport model is used to simulate the gradients corresponding to a given estimate of the emissions.

The atmospheric inversion theory relies on a statistical framework which accounts for the uncertainties in the prior estimate of the emissions, in the transport model and in the measurements, and which diagnoses the uncertainty in the estimate of the inverted (“posterior”) emissions as a function of the observation location and time, of the atmospheric transport, and of these prior, model and measurement uncertainties. This diagnostic is used in this study as a natural indicator of the inversion performance. Since it depends neither on the actual value of the observations that are assimilated, nor on the actual value of the prior estimate of the emissions, nor on the actual value of the corrections applied by the inversion on the prior emission estimates, it allows conducting OSSEs without generating synthetic gradient observations for the hypothetical networks that are tested and without conducting practical emission estimates.

2.1 Theoretical framework of the Bayesian inversion

By Bayesian inversion, the information from an observation vector \mathbf{y} of CO₂ concentration gradients is combined with a prior estimate \mathbf{x}^b of the CO₂ emissions budget for various

sectors, areas and time windows (i.e. of the vector of parameters controlled by the inversion \mathbf{x} , or “control vector” hereafter) to provide an updated estimate of the control vector \mathbf{x}^a (Enting, 2002):

$$\mathbf{x}^a = \mathbf{x}^b + \mathbf{B}\mathbf{H}^T(\mathbf{R} + \mathbf{H}\mathbf{B}\mathbf{H}^T)^{-1}(\mathbf{y} - \mathbf{H}\mathbf{x}^b), \quad (1)$$

where \mathbf{H} is a linear matrix operator linking \mathbf{y} with \mathbf{x} based on the modeling of the spatial and temporal distribution of the emissions at high resolution and the modeling of the atmospheric transport at high resolution. The uncertainties in \mathbf{y} , \mathbf{H} and \mathbf{x}^b are assumed to have statistical distributions that are Gaussian, unbiased and independent of each other. The linking of \mathbf{y} with \mathbf{x} in general suffers from some deficiencies in the measuring instruments and the atmospheric modeling. The sum of the measurement and model errors is called the observation error whose covariance matrix is denoted \mathbf{R} . We denote \mathbf{B} the error covariance matrix for the prior estimate of the control parameters. The uncertainty in the estimate \mathbf{x}^a given by (Eq. (1)) is Gaussian and unbiased and its covariance matrix (which is “smaller” than \mathbf{B}) is:

$$\mathbf{A} = (\mathbf{B}^{-1} + \mathbf{H}^T\mathbf{R}^{-1}\mathbf{H})^{-1}. \quad (2)$$

The comparison between this posterior error covariance matrix and the prior one, starting from realistic prior and observation error statistics, allows us to quantify the inversion performance. We pay a specific attention to the diagnostic of the relative difference between the posterior and the prior uncertainties for the total and sectoral budgets of the emissions during the month of January 2011.

In the following sections, we detail each component of our inversion system underlying Eq. (2) (see Fig. 1).

2.2 Control vector

Our control vector \mathbf{x} does not directly contain emission budgets, but rather scaling factors that are to be applied to the emission budgets which are included in the observation operator \mathbf{H} . For the sake of simplicity, Fig. 1 presents the inversion framework as if the emission budgets themselves were controlled, which is quite equivalent to the strict implementation of the inversion system. Each scaling factor in \mathbf{x} corresponds to the emission budget of a given spatial area of the IDF domain, a given temporal window, and a given sector or group of sectors of CO₂-emitting activity. The corresponding ensemble of areas, temporal windows

1 and sectors partitions the IDF domain, the month of January 2011 and the full range of
2 emitting activities respectively. Hereafter, we will call “control tile” the combination of an
3 area, a temporal window and a sector (or group of sectors) associated with a control
4 parameter.

5 While it is desirable to solve for the emissions at high spatial, temporal and sectoral
6 resolution, computational constraints, such as the inversion of \mathbf{B} and $(\mathbf{B}^{-1} + \mathbf{H}^T \mathbf{R}^{-1} \mathbf{H})$ in Eq.
7 (2) and the computation of \mathbf{H} which requires in principle as many transport simulations as
8 control parameters, limit the size of the control vector \mathbf{x} . We group the various sectors
9 provided by inventories (detailed in Sect. 2.4.1) into seven groups of sectors (see Appendix A
10 for details), namely 1) commercial and residential building heating/cooling, 2) road transport,
11 3) energy production (power plants), 4) combustion and production processes in industries, 5)
12 combustions from agricultural activities, 6) airline traffic, and 7) the remainder of all other
13 sectors with smaller emission budgets (e.g. railway, navigation, fugitive emissions, and
14 several minor production processes). These seven sectors are labeled for short as building,
15 road, energy, production, agriculture, airline, and remainder, respectively.

16 In order to save computations, for the less important sectors (isolated energy and production
17 point sources, agriculture, airline and remainder), we consider that the spatial area of control
18 for the inversion is the whole IDF area. However, for building and road emissions, we
19 spatially partition IDF into five zones for which the fluxes can be optimized: a central zone
20 (approximately the administrative definition of the city of Paris, which is very densely
21 populated) and four surrounding areas (the North-West, South-West, North-East and South-
22 East areas of the remaining IDF region, with borders adapted to the distribution of the
23 building and road emissions, see Fig. 2).

24 Regarding the temporal partitioning, for the three sectors which have the smallest budgets of
25 emissions (agriculture, airline, and remainder), the temporal resolution of the control vector is
26 daily. For the four other sectors (building, road, energy and production), we refine the
27 temporal resolution to 12h and control separately the daytime (7–19h) and night-time (19–7h)
28 emissions for each day, in order to account for the large diurnal variations in the emissions.

29 Atmospheric CO_2 observations are sensitive to vegetation-atmosphere CO_2 fluxes in addition
30 to fossil fuel CO_2 emissions. For cities surrounded by vegetation or containing green areas,
31 the impact of vegetation-atmosphere CO_2 fluxes on city carbon balance can be significant. For
32 instance, Nordbo et al. (2012) extrapolated from their measurements, that an 80% green-area

fraction would approximately make cities carbon-neutral. In our inversions, we account for the influence of the natural vegetation and soil CO₂ fluxes (or Net Ecosystem Exchange, NEE) by including, in the control vector, the scaling factors for the budgets of NEE in the full modeling domain (see Sect. 2.4) and for the four different 6-hour windows of the day (i.e. 0-6h, 6-12h, 12-18h, and 18-24h local time) over different 5-day periods during January 2011. The number of NEE scaling factors included in the control vector is thus 24, and the total number of scaling factors is 834 (see Table 1 for details).

2.3 Observations

We use an inversion system similar to that of B15, in which observations are taken to be CO₂ atmospheric concentration gradients between upwind and downwind stations (see Sect. 2.4.3 for details). The use of concentration gradients rather than concentrations well cancels out the pervasive large scale influence from remote fluxes outside of the city domain and informs about the local emissions between upwind and downwind stations. B15 also suggested assimilating only afternoon gradients when the wind speed is above a given threshold. By selecting afternoon gradients, we avoid biases in the vertical mixing during nighttime, mornings and evenings when mesoscale transport models have difficulties in representing the planetary boundary layer (Seibert et al., 2000; Steeneveld et al., 2008). Selecting data for high wind speed limits the signature in the atmospheric measurements of local sources that are in the vicinity of the measurement sites and that cannot be represented correctly by the transport model.

For investigating the potential of the inversion as a function of the observation network, we consider three strategies to deploy a given number of stations. These strategies define three corresponding types of networks: the Elliptical (E), Uniform (U) and Random-even (R) networks (Fig. 3). The E networks surround emissions in the city center, and appear suitable to the assimilation of city downwind-upwind gradients. The E networks consist in three concentric ellipses or rings of stations around the main part of the Paris urban area (the Paris administrative city and its 3 surrounding administrative circumscriptions), encompassing almost the whole urban area of IDF. The U networks position the stations on a regular grid. The R networks aim at balancing the position of stations near the city center and in the surrounding areas. The R networks have thus denser coverage over the city center and fewer stations in the surrounding zones than the U networks, but they still cover the whole IDF

domain. Apart from the E networks, the U and R networks have stations both close to the emissions in the Paris urban area and in rural areas in its vicinity.

We assess the potential of the inversion when using these networks of either 10, 30, 50, or 70 stations. For a given network, the station locations are chosen as a sub-set of a predefined set of 90 candidate locations, depending on the type of network. For example, 14, 24 and 52 of the 90 candidate stations for R networks are located in the urban center, the suburban area, and the rural area respectively. For a given number of stations n , 10 networks are selected for the inversion out of an ensemble of 100 networks that are generated by randomly selecting n stations from the set of 90 candidate locations. The selection of such sets of 10 networks is based on ad hoc verifications that the station locations should be evenly distributed in the urban, suburban and rural areas as would have been done for the design of real networks. This selection limits the range of the random generation of networks to a set of sensible networks for which a further discrimination should rely on the type of network performance assessment that is conducted in this study. Fig. 4 shows an example of an R network of 10 stations resulting from the above selection procedure. The design of current real city networks is much influenced by administrative and technical issues (e.g. agreements with potential hosts of the site and ability to fix inlets at desired height). Here we simplify such considerations and assume that the measurements are taken at 25 meters above ground level (magl) at all stations as discussed in more details in Section 2.4.3.

The strategy to properly combine stations from the different selected networks for city downwind-upwind gradient computation (and thus for the precise definition of the observation vector) is detailed in Sect. 2.4.3 as part of the description of the observation operator.

2.4 Observation operator

The observation operator \mathbf{H} that links the scaling of surface emission budgets to CO_2 concentration gradients in the atmosphere can be decomposed into a chain of three operators ($\mathbf{H} = \mathbf{H}_1\mathbf{H}_2\mathbf{H}_3$; Fig. 1): the spatial and temporal distribution of the CO_2 fluxes within a corresponding control tile \mathbf{H}_1 , the atmospheric transport of CO_2 given these spatial and temporal distributions of the fluxes \mathbf{H}_2 , and a sampling of the resulting simulated CO_2 to be compared with the observations \mathbf{H}_3 .

\mathbf{H}_1 maps the scaling factors in the control vector to the CO_2 fluxes on the transport modeling grid. It uses an emission inventory and an ecosystem model simulation to prescribe the small-scale spatiotemporal distribution of the gridded CO_2 fluxes. Applying \mathbf{H}_1 to a scaling factor uniformly rescales the prescribed CO_2 fluxes within each control tile, and thus adjusts the emission budget of that control tile. \mathbf{H}_2 is the mesoscale atmospheric transport model that maps the gridded fluxes generated by \mathbf{H}_1 to simulations of the CO_2 concentration fields on the transport model grid (at 2 to 10 km horizontal resolution and 1h temporal resolution, for a Northern France area encompassing the IDF region). \mathbf{H}_3 is a linear algorithm that computes Paris downwind-upwind CO_2 gradients between measurement stations, extracting the observations from the CO_2 field simulated by \mathbf{H}_2 .

2.4.1 \mathbf{H}_1

The NEE simulations from C-TESSEL – the land surface model of the short-range forecasts of the European Centre for Medium range Weather Forecasts (ECMWF) at a spatiotemporal resolution of 15 km and 3 h (Boussetta et al., 2013) – is interpolated to derive the distribution of NEE at the spatiotemporal resolution of the atmospheric transport model.

We rely on an inventory of the French emissions from the Institute of Energy Economics and the Rational Use of Energy (IER) at the University of Stuttgart to derive the distribution of sectoral fossil fuel CO_2 emissions in IDF at a high spatial resolution of $1 \text{ km} \times 1 \text{ km}$ (Latoska, 2009). It disaggregates the annual emissions of France in 2005 (according to the national inventory submissions 2007 from UNFCCC, <http://www.unfccc.int>), making use of extensive data from diverse databases for point, line, and area emissions, and of proxy information such as population and land cover maps. As for the temporal distribution of the emissions, we apply monthly, weekly and hourly temporal profiles also produced by IER, to derive hourly emission maps. These temporal profiles are defined for France as functions of each sector but not of the spatial location.

There are 51 sectors indexed by NFR code in the IER inventory. We compute the emission budgets for all these 51 NFR sectors, and re-aggregate them into the seven groups of sectors defined in Sect. 2.2 (see Table A1). The emission budget of the three major sectors (energy, road, and building) represents ~84.4% of total fossil fuel CO_2 emissions over IDF according to the IER inventory. Fig. 2 shows, for the seven sectors, the spatial distribution of the emissions among the 5 distinct geographic zones of IDF that are used to define the control

1 tiles. The northwest and southeast zones have more emissions than the other three zones,
2 mainly due to the presence of large point sources, e.g. the EDF power plants and the TOTAL
3 Grandpuits refinery (see Fig. 2 and Fig. 5c). Building and road emissions, on the other hand,
4 are distributed rather evenly in space over the five zones. The budgets of the emissions related
5 to production (7.4% of total), agriculture (3.7%), airline (3.3%) and remainder sectors (1.2%)
6 are relatively small compared to that of the first three sectors. Fig. 5 shows the spatial
7 distributions of the emissions from the seven sectors derived for January based on the IER
8 inventory and on the temporal profiles from IER. The IER inventory is not fully faithful to the
9 actual emissions from IDF, but in principle, this has very limited impact on the theoretical
10 computation in our OSSE framework of inversion.

11 2.4.2 H₂

12 Following B15, we use the mesoscale atmospheric chemistry-transport model CHIMERE
13 (Menut et al., 2013) to simulate the signature of CO₂ fluxes in the atmosphere over the IDF
14 area. This model has successfully served for air quality applications in megacities (Couvidat
15 et al., 2013; Zhang et al., 2013). The CHIMERE model domain in this study, which is the
16 same as that in B15, covers an area of about 500 x 500 km² in northern France that is centered
17 on IDF. Its horizontal resolution is 2 km × 2 km over IDF and its vicinity, and 2 km × 10 km
18 to 10 km × 10 km over the rest of the domain (see supplementary Fig. S1). In total, there are
19 118 x 118 cells in the model horizontal grid. Vertically there are 19 sigma-pressure (terrain-
20 following) layers from the surface up to 500 hPa. The top level of the first layer is at about
21 25 magl, and there are at least 6 layers below 250 magl. The meteorological fields driving the
22 CHIMERE simulations come from the ECMWF analyses at 15 km resolution. The
23 CHIMERE modeling system prepares meteorological data on its model grid by diagnosing
24 sub-grid processes, such as turbulent mixing and convection (Menut et al., 2013). We use
25 Global Land Cover Facility (GLCF) land use data at 1 km x 1 km resolution for such
26 diagnosis. Simple urban parameterization is adopted to correct wind speed in the surface layer
27 taking into account the increased roughness in the urban area (Menut et al., 2013), since B15
28 found no significant differences in the simulation of CO₂ mole fractions when advanced urban
29 scheme is used.

30 The exchange of CO₂ between the CHIMERE 3D regional domain and the surrounding
31 atmosphere depends on the wind conditions from the ECMWF product and the CO₂
32 concentrations at the domain boundaries. These exchanges characterize the signature of

remote fluxes outside the modeling domain that impact the observed and simulated atmospheric CO₂ in IDF. We need to account for these CO₂ boundary concentrations and for the CO₂ concentration field at the initial date of the simulations (i.e. the CO₂ initial condition) when simulating concentrations, which is not the case when applying the analytical computation of the uncertainties in the inverted emissions budgets through Eq. (2). When simulating CO₂ concentration fields for the preliminary illustration of the CO₂ variations in IDF in Sect. 2.4.3, the boundary conditions are derived from the interpolation of the global inversion product of Chevallier et al. (2010). This product has a resolution of 3.75° (longitude) × 2.5° (latitude), which gives about 2-3 cells at each CHIMERE domain lateral boundaries, yielding a smooth influence in both space and time from the CO₂ boundary conditions. The CO₂ initial condition is built from the interpolation of CO₂ given by that global inversion product. We do not control these CO₂ boundary and initial concentrations in our inversion system which explains why these components do not appear in the computation of the posterior uncertainties given by Eq. (2). However, as detailed in Sect. 2.5.2, uncertainties in these conditions still impact the accuracy of the inversion and have to be accounted for in the model uncertainty. Anthropogenic emissions within the modeling domain but outside IDF are not estimated in our inversions.

2.4.3 H₃

For a given network, the operator **H₃** consists in a combination of three operations: the linear interpolation of concentrations from the transport model grid to the actual point at which CO₂ measurements are collected, the selection of afternoon CO₂ concentration data (12-17h) at each station (upwind or downwind) when the wind speed from the transport model is higher than 3 m s⁻¹ at the downwind station, and the CO₂ city downwind-upwind gradient computation. While B15 consider gradients between pairs of stations downwind and upwind the full Paris urban area, this study assesses the potential of assimilating gradients between stations that are located within either urban or rural area. The gradients are thus representative of local urban emissions, and not necessarily of the citywide emissions as in B15. The assimilation of all gradients should help better constrain the spatial and sectoral distribution of the emissions.

In this synthetic study, we assume that the measurements are taken continuously at the height of 25 magl at all stations during the month of January 2011. This height can correspond to the setup of these stations at the top of existing buildings for which 25 magl is a common height

1 in the Paris area. The deployment of large networks with up to 70 stations at this height would
2 thus not have to rely on new infrastructures as if the targeted sampling height was
3 significantly higher (which would be a critical barrier for the practical implementation of the
4 network). Local sources and transport that are poorly represented with a 2 km resolution
5 model may have large impact on the concentration measurements at such a height. However,
6 all real data assimilated by B15 were sampled at peri-urban stations at less than 25 magl. By
7 selecting the data during the afternoon only and for high wind speeds, B15 limited such a
8 local impact. Furthermore, their diagnostic of the model error which is used to set-up the
9 OSSEs in this study (see Section 2.5.2) implicitly accounted for this impact. Still, assimilating
10 25 magl measurement in the core of the urban area (which corresponds to a significant
11 number of the hypothetical sites investigated in this study) is likely challenging due to the
12 high density of strong sources and to the complexity of the urban canopy, and had not been
13 attempted by B15 even though they derived typical estimates of the model error for urban
14 measurements (see Sect. 2.5.2). This will be further discussed in Sect. 4.

15 The CO₂ gradient computation demands selecting pairs of upwind and downwind stations.
16 For each observation at a given time, the station at which that observation is made is first
17 considered to be a downwind station. We then select, for that observation, a matching
18 observation at an upwind station, based on the wind direction at the downwind station (given
19 by the ECMWF meteorological data, also used to drive the CHIMERE model). We impose
20 that the angle between the direction from the upwind to the downwind stations and the wind
21 direction at the downwind station is comprised between $\pm 11.25^\circ$. The choice of such a range
22 of angles for the gradient selection is a trade-off between the need to select enough data to
23 constrain the inversion, and the need for ensuring that we do not depart too much from the
24 objective of assimilating “downwind-upwind” gradients. It is derived from the study of
25 Staufer et al. (2016) who analyzed the impact of such a choice on the results of the inversion
26 when using real data. Fig. 4 illustrates the principle of the gradient selection by showing the
27 wind direction for a downwind observation and the area that covers its corresponding upwind
28 stations.

29 We further impose that the distance between the upwind and downwind stations should be
30 larger than 5 km (to avoid assimilating gradients that are mostly representative of local
31 sources) and as close as possible to 10 km. This 10 km distance would correspond to the
32 advection of an air parcel during 1 h with a wind speed of 3 m s^{-1} (i.e. our threshold on the

wind speed for the assimilation of gradients). Here, the gradient computation in the reference inversion ignores the time lag needed to advect an air parcel from upwind to downwind stations and it is based on the difference between simultaneous hourly mean observations. This explains why the 10 km distance is seen as a good trade-off between the need for being representative of large scale emissions and the need to limit the impact of ignoring the time required for transporting air masses from an upwind to a downwind site. We discard the downwind observations for which no upwind station can be found based on our selection rules. About 7-16% of total observations are retained for gradient computation with this data selection procedure, depending on the size and type of the networks.

Fig. 6a shows statistics on the afternoon hourly wind conditions at an example station EVE26 during January 2011, and Fig. 6b shows restriction of this statistics to the wind conditions at EVE26 when EVE26 is selected as a downwind site for gradient computation. Winds at station EVE26 blow prevailing along the southwest-northeast direction for this period (Fig. 6a). Since EVE26 is located to the northeast of the urban center (Fig. 6c), the corresponding upwind stations for gradient computation are mostly selected in the southwest direction (Fig. 6b-c).

As the observation operator is linear, one can evaluate the contribution of a flux component to the CO₂ mixing ratio at the measurement stations by applying the observation operator to that specific flux component, cancelling all other flux components. We thus perform eight CHIMERE simulations with, in input, respectively the simulation of the NEE in Northern France and the inventories for the 7 sectors of the fossil fuel emissions in IDF described in Sect. 2.4.1 to evaluate the contribution of these different types of flux to the CO₂ variations during January 2011 at the hypothetical station locations considered in this study. This corresponds to applying \mathbf{H} to control vectors with scaling factors corresponding to the NEE or to a specific sector of emission set to 1 and others to 0 and ignoring CO₂ boundary conditions. Fig. 7 plots the time series of CO₂ mole fractions corresponding to the different types of flux at 10 stations of an R network (which are indicated by red triangles in Fig. 4) including 2 urban stations (EVE07 and EVE11 in Fig. 6c) and 8 rural stations.

CO₂ series from Northern France NEE in January have small daily variations compared to that of CO₂ from the fossil fuel emissions in IDF and show very similar patterns at all the ten stations. During night-time, CO₂ emitted by the ecosystem respiration or by the anthropogenic activities is trapped within the usually stratified nocturnal planetary boundary layer, which

generates peaks in the CO₂ time series. However, as explained in Sect. 2.3, the representation of the night-time variations (in particular of their amplitude) by the transport model is not reliable. The diurnal variations of CO₂ are driven by the diurnal variations of the NEE (with a sink of CO₂ due to photosynthesis during daytime), the CO₂ emissions from major sectors (building, road and energy), and the meteorology within the planetary boundary layer.

There are strong positive CO₂ concentration gradients between the urban-urban and urban-rural pairs of stations when analyzing the signature of the major sectors of anthropogenic emissions (Fig. 7). Fig. 7i shows histograms of simulations of the concentration gradients corresponding to the observation vector when using this 10-stations R network for inversion. These simulations are obtained by forcing CHIMERE with the estimates of the total NEE and anthropogenic emissions described in Sect. 2.4.1 (i.e. by applying **H** to control vectors with all scaling factors set to 1 and accounting for the CO₂ boundary conditions described in Sect. 2.4.2). The three different histograms contain the gradients between 2 rural, 2 urban or 1 rural and 1 urban station, respectively. All the concentration gradients between downwind urban and upwind rural stations are positive, carrying a mean CO₂ gradient of ~14 ppm with a standard derivation of ~4 ppm. In contrast, the concentration gradients between downwind rural and upwind urban stations have 20% negative values, with a mean of ~3 ppm and a standard deviation of ~7 ppm. The gradients between rural downwind and rural upwind stations have a mean of ~5 ppm, a standard derivation of ~7 ppm, and ~13% negative values. Most of these rural-rural negative gradients were found at station pairs where the upwind rural station is much closer to the city center than the downwind rural station (e.g. EVE34 and EVE85 whose distance is ~23 km). Ignoring the time lag that is required for an air parcel to be transported from the upwind to the downwind stations when computing the CO₂ gradients explains a large portion of these negative gradients. The emissions vary in time, and, at a given time, the upwind rural station can bear a signature of a peak dominated by the emissions from the upwind nearby city center while this signature has not reached the distant downwind rural station yet. Occasional changes in the wind directions between the upwind to the downwind stations may also explain that, sometimes, air masses reaching the downwind stations have not necessarily been transported over the areas with high fossil fuel emissions.

2.5 Accounting for uncertainties

2.5.1 Prior uncertainties

Formal statistical methods, such as Monte Carlo approaches, can be used to estimate errors due to uncertain activity data and emission factors and thus the overall uncertainties in inventories at the global/national scale (Fauser et al., 2011; Wang et al., 2013). However, to our knowledge, there are currently no studies evaluating uncertainty in existing inventories at the city scale. B15 used the AIRPARIF 2008 inventory as a prior emission estimate for their inversions, and assigned a 20% 1-sigma uncertainty in the monthly estimate of the total emissions from IDF. Following B15, we set a prior 1-sigma uncertainty of about 20% in monthly total emissions from the Paris metropolitan area. In practice, few cities benefit from such high resolution local inventories (Appendix A), and the setup of the prior uncertainties for other cities may have to be higher since the quality of the prior knowledge from their available inventories is not as good.

We assume that there is no correlation between the prior uncertainties in the emission budgets (and thus in their scaling factors) for different sectors of emissions (see Fig. 8a). For a given sector, the correlations of the uncertainties in scaling factors for different areas and time windows are given by the Kronecker product between spatial correlations (if there are different control areas for this sector) and temporal correlations. We set a value of 0.6 for the spatial correlations between prior uncertainties in scaling factors for building or road emissions that correspond to two different geographical areas (Fig. 2). The temporal correlation of the prior uncertainties in scaling factors is modeled using an exponentially decaying function with a characteristic correlation length of 7 days for each sector (Fig. 8a). Uncertainties in individual scaling factors for a given control tile are derived based on this configuration of the correlations and on the two following assumptions: (1) the aggregation of uncertainties in all the individual scaling factors leads to an overall 20% 1-sigma uncertainty in total emissions for January 2011, and (2) the 1-sigma uncertainties for the budget for January 2011 of the seven sectors of emissions are approximately equal to one another. The latter assumption is supported by a recent census, which was conducted by National Physical Laboratory (NPL) based on a group of 26 city inventories reported to the carbonn Climate Registry (cCR) suggesting that the data collected for different sectors can actually have a similar level of quality (report available from www.carbonn.org). The sensitivity of the inversion results to the configuration of **B** and thus the robustness of the inversion are

discussed in Sect. 4. By construction, the resulting 1-sigma uncertainties in the budgets for the seven sectors of emissions are larger than that in the total emission estimate. They are approximately equal to 36% (Fig. 9). As B15, we set a prior uncertainty in the NEE scaling factors of about 70%.

Controlling large control tiles with a single scaling factor does not mean that the uncertainties in the emissions at higher resolution are assumed to be entirely correlated within a control tile. The uncertainties in the distribution of the emissions at higher resolution given by the observation operator must actually be accounted for in the computation of the observation error as indicated in the following section. This part of observation error is generally called the aggregation error.

2.5.2 Observation uncertainties

Observation uncertainties arise from both the measurement errors and the model errors associated with the observation operator (including the transport model errors). The precision of the instruments presently used (typically cavity ring down spectrometers) for the climate studies can have a high precision that is better than 0.1 ppm (1-sigma) on hourly mean data. When properly calibrated, typically every 2 weeks to 2 months, these high precision instruments do not bear any significant drifts or biases, and the systematic errors borne by their hourly measurements are smaller than 0.13 ppm. This level of measurement error is negligible compared to the current transport model errors that are detailed later in this section. Even though the deployment of dense networks with up to 70 sites would rely on LCMP sensors and on a different calibration strategy, we conduct the main inversion experiments assuming that they would measure CO₂ with a precision and accuracy still negligible compared to the model error. However, some sensitivity tests will be performed to assess the impact of much larger measurement errors (Sect. 3.2).

The model error, which applies to “downwind-upwind” CO₂ gradients in this study, is mainly a combination of the aggregation error due to uncertainties in the spatial and temporal distribution of the fluxes within a control tile that is not resolved by the inversion, of the representativeness error (the difference in terms of spatial representativeness between the measurements and the CO₂ simulated with a 2 km to 10 km horizontal resolution model), of the atmospheric transport modeling error, and of the errors in the model CO₂ initial and boundary conditions.

Following B15, we assume that the observation error covariance matrix \mathbf{R} is diagonal, which means that the model errors for the CO₂ gradients are not correlated in time or in space. This implies that there is no correlation of the model errors in the direction orthogonal to the wind (see later in this paragraph for a discussion about the direction parallel to the wind). Based on statistics on the model-measurement misfits, B15 diagnosed the total model error when simulating CO₂ hourly concentrations at individual urban and rural sites and for hourly city downwind-upwind gradients between rural stations. They found that this error is of the order of 5 ppm and 10 ppm for hourly CO₂ data at rural and urban stations respectively, and of 3 ppm for hourly gradients between rural stations. The high model error at individual stations characterizes the difficulties of atmospheric models to represent the CO₂ transport within and in the vicinity of urban areas, even when selecting data during the afternoon and for high wind speed only. B15 explain the smaller model errors for gradients than for individual CO₂ data by the high spatial correlations between model errors at upwind and downwind sites. These spatial correlations are due to the large spatial coherence of the errors from the model boundary conditions along the wind direction, whose cancelling is the main aim of the gradient computation. In principle, this is not incompatible with the assumption mentioned above that there is no correlation of model errors in the direction orthogonal to the wind since it bases on the idea that the correlation follows the advection of air parcels and of the atmospheric signature of remote sources and sinks. Still, the diffusion of the signature of remote sources and sinks through their atmospheric transport could correlate the model error between different gradients corresponding to close locations. Characterizing such spatial correlations is very challenging and falls beyond the scope of this paper.

The diagnostics of model error by B15 account for the transport and representativeness errors and of errors in the CO₂ initial and boundary conditions of the same transport configuration as that used in our study. It also accounts for aggregation errors since their inverse modeling framework solves for emissions at a coarser resolution than in this study (they apply scaling factors for the 6-hour mean budget of the emissions in IDF). Smaller aggregation errors should apply in our configuration but we conservatively use their diagnostic to assign the model errors in our OSSEs. This setup of the model errors in our study is also based on a simple derivation of the spatial correlations of the model error for individual measurements between upwind and downwind stations based on their results. This leads us to assign a standard deviation of 3.5, 5.6, and 7 ppm respectively for the observation error on gradients between rural stations, between rural and urban stations and between urban stations.

3 Results

3.1 Results with the reference inversion configuration

We conduct a series of inversions of sectoral and total emissions during the month of January 2011 using E-, R- and U-type networks with 10, 30, 50 and 70 stations. The inversion results are analyzed in terms of posterior uncertainties in the inverted fluxes and in terms of uncertainty reduction by the inversion (Fig. 9). The uncertainties discussed here are relative uncertainties, which are defined as the uncertainty budgets in percentage of the budgets of the corresponding emissions obtained from the IER inventory (and included in the observation operator).

With small E, R or U networks of 10 stations (i.e. the size of some of the existing networks), inversions are effective in reducing uncertainties in total emissions as well as in the emissions from the three major sectors (building, road and energy). The inversion on average reduces the 1-sigma uncertainty in the total emissions estimates from ~19% a priori down to ~11% a posteriori (a 42% uncertainty reduction). The 1-sigma uncertainties in building, road and energy emission estimates are reduced on average from ~36% (prior uncertainty) down to about 23%, 27% and 24% respectively (about 35%, 23% and 31% uncertainty reduction respectively over the prior uncertainty). In contrast, the uncertainty reduction is very limited for emissions from agriculture, airline, production, and remainder sectors. However, the contribution of these four sectors of emissions to the total budget is rather small, and represents only ~16% of the total emissions in IDF according to the IER inventory (Fig. 9e).

In order to limit the influence of specific station locations and to weight the sensitivity to the network design (and thus the need for network design studies), we performed inversions with 10 random networks of the same type and size. These random networks differ from one another in their station locations, but still follow their respective network type (see Sect. 2.3 on how we generate these random networks). The variation (error bars in Fig. 9) of the inversion performance due to changes in the station locations is in general small, compared to the variations due to the changes of the network type and size (see Fig. 9). The influence of the station location is large for the agriculture sector, but emission budget for this sector is small.

The uncertainty reduction increases with larger networks. However, this increase generally slows down and is rather weak once the networks have more than 30 stations (Fig. 9a-c). While there is not much difference between the uncertainty reduction for energy emission

estimates when using 30-station or 70-station E networks (Fig. 9a), the increase in uncertainty reduction for building emissions when using 70-station compared to 30-station U networks is still significant. To further illustrate this slowdown effect, we assess the number of Degrees of Freedom for Signal (DFS; Rodgers, 2000) for inversions using different networks (Fig. 10a). The DFS characterizes the number of independent pieces of information brought by the observations and therefore the relative weight of the signal from the observations against the noise from the observations in the analysis. If the uncertainty in the measurement is very high or if the measurements bring redundant information, the measurements will provide a small DFS. In practice, the overall DFS is the trace of matrix $(\mathbf{B} - \mathbf{A}) \mathbf{B}^{-1}$ and has a value between zero and the number of observations d (Wu et al., 2011). For our Paris case study, we find that the DFS per concentration gradient observation (i.e. the ratio DFS/d) is less than 10%, that is, only a small percentage of observations are effectively assimilated and correspond to the signal but not the noise. Such small DFS results from the diffuse nature of atmospheric transport (which weakens the atmospheric signature of the emissions from specific sources and spreads it throughout the different concentration gradients) and from the uncertainty in atmospheric modeling (which weakens the constraint given to observations during the inversion analysis). When using denser networks, the DFS per observation decreases, and the information brought by the different gradient observations on the budgets of sectoral or total emissions over the full IDF area has more redundancy. This is due to the decrease of the distances between the upwind and downwind stations, and between the different upwind (or downwind) stations that are selected for gradient computations. Despite such a densification of the network, many isolated and local sources, which dominate some sectors of emissions, are yet difficult to catch, in particular with our 5 km threshold on downwind-upwind site distance (see Sect. 2.4.3). Additionally, the selection of daytime observations for high wind speed dramatically reduces the observational constraint on the emissions at other periods of time (see Sect. 2.2 for the temporal discretization of the control vector), which, altogether have a large weight on the total emission budget. Therefore, the slowdown of the uncertainty reduction when using larger networks is also explained by their convergence to a value which reflects this lack of constraint.

The 1-sigma posterior uncertainties obtained with 70-station networks of type either E, R or U are on average 32%, 33%, 18% and 31% smaller than those obtained with 10 stations for building, road, energy and total emission estimates respectively (Fig. 9a-c). Compared to the prior uncertainties, inversions with 70-station networks achieve an uncertainty reduction of

60% on average for the total emissions which leads to an 8% 1-sigma posterior uncertainty. In contrast, the 1-sigma posterior uncertainties in building, road and energy emissions are 16%, 18% and 20% respectively, with uncertainty reductions by 56%, 48% and 43% respectively compared to the corresponding sectoral prior uncertainties. Large networks are more promising for the estimation of dispersed surface emissions such as those from the building sector.

Different types of networks show distinct ability for monitoring emissions, which is usually sector-specific. For instance, using a U- instead of a E-type 70-station network leads to 18% vs. 22%, 18% vs 19%, 15% vs. 18%, and 6% vs. 9% differences in the posterior uncertainty in the estimates of the energy, road, building and total emissions (Fig. 9d). Compared to the U networks, the E networks result in larger DFS values (Fig. 10a) but worse performances in uncertainty reduction for total emission estimates (Fig. 10b). The stations in the E network are around the area of high emissions (in particular central Paris), therefore their concentration gradients would be overall more sensitive to the nearby emissions (hence with larger DFS values). However, focusing only on central Paris makes the E network less efficient for controlling the emissions in the rural area (see the spatial distribution of the energy, building and road emissions in Fig. 5a-c). This is because there are large point sources (e.g. the EDF Porcheville power plant and the TOTAL Grandpuits refinery from the energy sector; Fig. 2) and considerable building emissions located outside of the largest ring of the E networks (Fig. 3 and Fig. 5).

In all experiments, the prior and posterior relative uncertainties in sectoral budgets are higher than that in the total emissions due to the fact that the sectoral budgets from inventories or atmospheric inversions are based on a mix of independent information and on the split of the information on the total emissions (which is characterized by null or negative correlations between the uncertainties in the different sectors). The analysis of the negative correlations between posterior uncertainties in different emission budgets is indicative of the capability of the inversion system to well spread the attribution of an overall concentration increase between them (Fig. 8). Large negative correlations associated with high posterior uncertainties indicate that the posterior uncertainties in the individual budget for the different corresponding emission components arise from improper attributions of budget among these emission components while the sum of the emissions budget of all components may be well constrained by the inversion. The skill of the larger U networks for separating the sectoral

emissions budgets is higher than that of the smaller U networks and than that of the equal-sized E networks (see Fig. 8b-d for cross correlations between building, road, and energy sectors).

However, the E networks perform better than the U networks for estimating emissions from the airline sector. This is due to the fact that airport emissions (see Fig. 2 and Fig. 5f) are located between the two outer rings of the E networks. Moreover, the E networks perform well to reduce uncertainty in road emission estimates, although a significant portion of the road emissions occur in rural areas that are not covered by the E networks. This is probably because (1) the smallest inner ring coincides with the heavy-loaded Paris peripheral boulevard (25% of the traffic in Paris); (2) the Paris road network (Fig. 5b) sprawls mainly in the urban and suburban area, which are comprised within the largest outer ring; and (3) the configuration of the E networks (as well as that of the R networks; Fig. 3) is better adapted than that of the U networks to distinguish between the signature of the road emissions and that of the other emission sectors.

3.2 Sensitivity to the measurement and model errors, and to the amplitude of the uncertainty in NEE

The results analyzed above are based on the reference inversion configuration detailed in Sect. 2. However, as introduced in Sect. 2.5.2, observation errors could be in practice larger than assumed, either because we would need to use LCMP sensors with smaller accuracy than the present high precision instruments in order to deploy dense networks, or because our assumptions regarding the model errors (derived from the diagnostics of B15 over a small number of sites) would not be adapted to dense measurement locations.

We have thus repeated the inversion tests with values for the observation error standard deviations inflated by 50% compared to those described in Sect. 2.5.2 for the reference configuration (which would corresponds to a dramatic increase of the measurement error or decrease of the modeling skills, see the discussion in Sect. 4). The 1-sigma posterior uncertainties resulting from inversions with inflated (Fig. 11) and reference (Fig. 9d) observation errors when using 70 sites and the type of network providing the best performances (depending on the sector) are (1) 7% and 6%, respectively, for total emission estimates with U networks, (2) 16% and 15%, respectively, for building emissions with U networks, (3) 19% and 18%, respectively, for road emissions with R networks, and (4) 20% and 18%, respectively, for energy emissions with U networks. The increase of the posterior

uncertainty in total emission estimates resulting from this inflation of observation error standard deviation is significant (typically 1% of the budget of prior total emissions). However, these increases are relatively modest compared to the typical variations of posterior uncertainties depending on the different networks that are tested. This is likely due to the fact that, at the monthly scale, the projection of the uncertainty in the prior emissions into the concentration space is very high compared to the observation errors, and to the fact that the observation limitation is primarily related to their spatio-temporal coverage rather than to the precision of the hourly measurements and of their simulation by the observation operator.

Our reference experiments apply to a month in winter, when the CO₂ signal from the NEE is low, and the heating emissions are high, which decreases the difficulty to separate it from that of the anthropogenic emissions in the concentration gradients. This could favor the monitoring of the anthropogenic emissions during this season. In order to assess whether the results obtained in this study can be indicative of the performance of the inversion during summer, when the NEE is higher (we ignore here the impact of the decrease in the heating emissions), we run inversions where the prior error standard derivation for the NEE fluxes is inflated/shrunk by 100%, or where the NEE fluxes within the observation operator \mathbf{H}_1 (see Sect. 2.4.1) are multiplied by 3 or 5 (which typically corresponds to the ratio between the NEE in July vs. January according to the C-TESSEL simulations). The differences between the uncertainty reductions for the total emission estimates obtained with the reference configuration and when applying these changes are found to be less than 1%. Actually, the correlation between the posterior uncertainties in the NEE fluxes and in the total and sectoral fossil fuel CO₂ emissions (except the building emissions) are nearly zero (Fig. 8b-d), which implies that the different networks are sufficiently dense to provide a clear separation between natural and anthropogenic fluxes within our inversion framework. This explains the weak influence of the prior uncertainty in the NEE for the estimate of the fossil fuel CO₂ emissions.

These sensitivity analyses strengthen the confidence in the robustness of our inversion results that are based on the experiments with real data of B15 and Staufer et al. (2016).

4 Discussions and conclusions

4.1 Summary with complementary analysis

We have developed an atmospheric inversion method to quantify city total and sectoral CO₂ emissions using networks of measurement sites within and around a city. This method combines a prior emission estimate from an inventory, with the information from

concentration gradient measurements (independent of the inventory) to provide updated emission estimates with reduced uncertainty. Such an inventory can be obtained for instance directly from local agencies or interpolated from regional inventories developed by public research establishments (see Appendix A). We examine the ability of this inversion system to reduce uncertainty in emission estimates for diverse emitting sectors of the Paris metropolitan area (~12% of France CO₂ fossil fuel emissions) as a function of the size and design (i.e. location of the stations) of the observation networks.

We perform inversions over a one-month winter period (January 2011) under a framework of Observing System Simulation Experiments, in which we test several types of theoretical networks of stations sampling CO₂ atmospheric concentrations at 25 meters above ground level. When using 10 stations, which is the typical size of the few current networks, the inversion considerably reduces the uncertainties in total emission estimates for January 2011 (by ~42%) from a ~20% 1-sigma prior uncertainty down to ~11% 1-sigma posterior uncertainty. The uncertainty reduction for sectoral budgets is also high but the 1-sigma posterior uncertainties for these budgets is ~25% i.e. more than twice as high as for total emissions. In the prior inventories as in our inversion experiments, the total emissions are better constrained (in relative terms) than the sectoral budgets. The inversion is more efficient in decreasing uncertainties in the budget of dispersed emissions from residential and commercial heating than that in other sectoral budgets. We observe significantly larger uncertainty reduction in sectoral emission budget estimates when using more stations. The decrease of the uncertainties in the inverted emissions when using 70 stations vs. 10 stations is of 32% for commercial and residential buildings, of 33% for road transport and of 18% for the production of energy by power plants, and of 31% for the total emissions, respectively. The three major sectors (building, road, and energy) cover most of the emission budget according to the IER inventory used in this study. Therefore, while the extension of the networks does not seem to be critical for the verification of the city emission total budgets, it likely provides high advantages for the monitoring of sectoral emissions. When using 70 sites, the 1-sigma monthly posterior uncertainty in the building emission estimates can be brought down to 15% while that for transport and energy emissions estimates is reduced to 18%.

4.2 Discussion on the levels of posterior uncertainties and on the relevance of the corresponding estimates

1 We can hardly determine whether the levels of precision in emission accounting obtained by
2 atmospheric inversions would be enough for a MRV framework since the MRV experiences
3 for citywide CO₂ emissions are still very limited (Appendix A). We still attempt at evaluating
4 the usefulness of estimates with these different levels of uncertainties. In MRV practice,
5 mitigation actions and climate plans are usually based on targets for the reduction of annual
6 budgets of the emissions and should thus be evaluated based on the monitoring of annual
7 budgets and/or of their trends. In this study, the accuracy of the inversion is analyzed for a
8 single winter month, and inversion experiments over longer time periods are out of the scope
9 of the paper (for reasons of computational cost). However, results from Sect. 3.2 indicated
10 that its accuracy in spring, summer and fall should be similar. In order to get an indication on
11 the accuracy of the inversion at the annual scale, we thus assume that the scores obtained here
12 apply to all months during the year, and use two opposed and extreme hypotheses regarding
13 the correlations between posterior uncertainties from month to month. The first one is that
14 these uncertainties are fully independent, which can be supported by the independence of the
15 measurements used to constrain the estimates from month to month. The second one is that
16 these uncertainties are fully correlated, which can be supported by the fact that part of the
17 posterior uncertainty is related to residual prior uncertainties that have not been decreased by
18 the inversion, and that the prior uncertainties can be highly correlated from month to month.
19 Actual correlations should lie between these two extreme cases. By doing so, we obtain a
20 simple, conservative and indicative assessment of a typical range of 2-sigma annual
21 uncertainties in the total and sectoral emission estimates from the inversion. With such a
22 conversion, the prior uncertainty in total emissions would range between 12% and 40% while
23 that in the sectoral budgets of the emissions would range between 21% and 72% depending
24 on the sectors. The 2-sigma annual posterior uncertainty in total emissions would range
25 between 4% and 23% when using 10 to 70 sites. The 2-sigma annual uncertainty in the
26 budgets for the three main emitting sectors (building, road, energy) would range between 13%
27 and 59% when using 10 sites, and between 9% and 44% when using 70 sites, while it would
28 systematically exceed 14% for the production sector even when using 70 sites. Such annual
29 uncertainty ranges vary a lot for the secondary sectors of emissions (airline, agriculture,
30 remainder) e.g. from between 7% and 41% for agriculture to systematically higher than 20%
31 for the remainder emissions when using 70 sites.

32 We compare these numbers to the diagnostic (based on expert judgments as well as error
33 propagation calculations with the IPCC Tier 1 method) of the typical uncertainty in the

national inventories in developed countries, which could apply to theoretical city scale inventories under MRV frameworks. The uncertainty in national inventories is country-specific, but for the seven Annex I countries surveyed by Pacala et al. (2010), the uncertainty in CO₂ fossil fuel emissions is consistently lower than 10% (2-sigma). For France, the uncertainty of the CITEPA national inventory (annually reported to UNFCCC) is estimated to be of 5% (2-sigma) for year 2012 according to CITEPA (2014). The uncertainty levels for estimates of emissions from different sectors can vary significantly at the national scale (Pacala et al., 2010; CITEPA, 2014). For instance, uncertainties for some activities such as mineral, metal and chemical productions are considerably larger than the 5% value for total emissions, but the share of these emissions in the total fossil fuel emissions is usually small. Uncertainties for other sectors are closer to 5% according to CITEPA (2014).

Furthermore, succeeding in delivering a 5% or 10% 2-sigma annual uncertainty for the total emissions of a city would translate into an ability to assess a 25% reduction of total emissions on a 15-year horizon at a 95% confidence level (detection interval [18%, 32%] or [11%, 39%] respectively, $p = 0.05$ for linear trends of emissions; see Appendix C for numerical details). The Paris climate plan for example, aims at reducing the GHG emissions by 25% by 2020 and by 75% by 2050 relative to the 2004 baseline (Mairie de Paris, 2012). This means that a 10% annual uncertainty would be enough to monitor the trend of Paris emissions over time.

Comparing our indicative estimate of the typical range of posterior uncertainties in annual total and sectoral emissions to these 5% and 10% 2-sigma uncertainties confirms the need for dense observation networks if willing to build a valuable MRV framework. A significant part of the range of posterior uncertainties derived for the annual total emissions when using 10 sites is below the 10% 2-sigma uncertainty. However, it does not reach the 5% 2-sigma uncertainty and most of this range is lying above the 10% 2-sigma uncertainty. When using more than 30 sites and U networks, the 5% 2-sigma uncertainty can be reached by the most optimistic estimates of posterior uncertainties in annual total emissions and most of their range lie below the 10% 2-sigma uncertainty. Furthermore, as far as the most optimistic derivation of annual results is concerned, inversions with more than 30 sites would be required to expect that the posterior uncertainties in annual emissions for the three major sectors can be close to 10% 2-sigma uncertainty. This level can be reached with U or R networks of more than 50 stations for building emissions, but it cannot be reached for the road and energy sectors. 70 sites are required to expect posterior uncertainties of less than 10% 2-

1 sigma uncertainty for all these 3 sectors at the annual scale. For the other types of sectors, the
2 inversion with U, E or R networks is likely not adapted to reach the 10% 2-sigma uncertainty
3 level at the annual scale.

4 With 70 sites, a significant part of the ranges of 2-sigma posterior uncertainties in annual
5 emissions for the three major sectors is below ~15% (for any type of networks). Such a 2-
6 sigma uncertainty at the annual scale still corresponds to an ability to detect the 25%
7 reduction of emissions on a 15-year horizon at a 95% confidence (detection interval [3%,
8 46%], $p = 0.05$ for linear trends of emissions; see Appendix C). The 5% and 10% 2-sigma
9 uncertainties can thus be viewed as stringent for the monitoring of sectoral emissions but the
10 comparisons to these levels of uncertainty indicate that dense networks would be necessary to
11 ensure that the inversion has a high potential to verify sector-wide mitigation policies/actions
12 or to check whether sectoral mitigation targets are fulfilled.

13 **4.3 Robustness of the inversion configuration and requirements on the model, methods** 14 **and instruments supporting such a configuration**

15 The results obtained in this study should not be over-interpreted, since (1) we worked under
16 synthetic settings for large city networks, and (2) the configuration of our inversion system
17 may fail to be fully faithful to reality (e.g. the idealized parameterization of the prior
18 uncertainties in scaling factors defined for different sectors and spatial zones, and of the
19 assumed independent errors in concentration gradient observations). Nevertheless our
20 inversions were based on the experience from B15 and Staufer et al. (2016) in which real data
21 from a few number of stations around Paris were used. In addition, we performed sensitivity
22 analyses by significantly inflating the observation error to account for a potential increase of
23 the measurement and modeling errors when deploying dense networks with many sites in the
24 core of the urban area, and this analysis gave confidence in the robustness of the results
25 obtained with our reference inversion configuration.

26 Our tests ignored potential temporal correlations in the model and measurement errors.
27 Increasing the standard deviation of the observation error for hourly data should have a
28 similar impact on results at the monthly scale as accounting for short temporal
29 autocorrelations (over timescales typically smaller than few days). Increasing the standard
30 deviation of the observation errors instead of modeling their autocorrelations is a common
31 technique in atmospheric inversion (Chevallier, 2007).

1 The results from B15 and Staufer et al. (2016) support the idea that the model has no major
2 biases or errors with large temporal correlations. However, even though B15 diagnosed model
3 errors for measurements in the core of the urban area, they and Staufer et al. (2016) did not
4 attempt at assimilating such measurements. We thus implicitly make the assumption that there
5 is no major model errors with long temporal correlations associated with high local sources
6 for 25 magl locations in the urban environment. This assumption is supported by the idea that
7 relevant investigations (mobile measurement campaigns, high resolution transport modeling)
8 can be led to avoid setting up sites close to such sources. In our study, the hypothetical
9 stations are all located without a precise definition of their specific position within the
10 2 km x 2 km grid cells of CHIMERE, which are sufficiently large to assume that they
11 encompass areas less prone to local sources. High resolution transport modeling can also be
12 used to develop techniques for filtering the signal from the large scale emissions against that
13 of local sources in the measurements.

14 The theoretical use of LCMP sensors to allow the deployment of networks of up to 70 sites
15 could be viewed as a source of systematic measurement errors with long temporal scales of
16 autocorrelation. Our results from Sect. 3.2 suggest that if the measurement errors are
17 significant and increase the observation errors by 50%, they can have a significant impact on
18 the accuracy of the inversion. Such an inflation of the observation error would result from
19 1 ppm systematic errors with 7 day temporal correlations in the hourly measurements (since it
20 would result in ~1.5 ppm systematic error in weekly mean gradients, or, if converting the
21 temporal correlations into an inflation of the hourly standard deviations, in an 8 ppm
22 measurement error for hourly gradients). Therefore, our sensitivity tests indicate that the
23 LCMP accuracy and calibration strategy should ensure that the systematic errors do not
24 exceed 1 ppm, and if they are close to this value, that they are not auto-correlated over more
25 than one week. This recommendation adds to the recommendation that the cost of LCMP
26 sensors should not exceed 1-5 k€ euros (see the discussion in Appendix B).

27 The choice to rescale the budgets of emissions over large areas and sectors rather than at high
28 resolution could make our results quite optimistic. However, the aggregation errors associated
29 with such a coarse scale rescaling are accounted for in the inversion. Furthermore, the
30 configuration of the networks tested in this study is adapted to that of the “control tiles” which
31 helps avoiding aggregation artefacts. With such configurations, the results show that having
32 as many sites as possible around the most prominent sources of a tile will give a better control

on the average budget of that tile. As would have been expected with a high resolution inverse modeling system, our coarse inversion system identifies the networks that can provide a strong constraint on most of the largest sources within the tiles, and it demonstrates some sensitivity to the network types and station locations.

The assumptions underlying our setup of the sectoral uncertainties (in particular for the prior error covariance matrix **B**) can definitely impact the results of the uncertainty reduction. It could raise some concerns regarding the analysis of the absolute values of uncertainty reduction for a given network. However, the comparative analysis of the uncertainty reductions when using different networks but the same inversion setup (i.e. the network design analysis) should bring more robust conclusions.

4.4 Perspectives

While the deployment of dense city networks of more than 30 sites seems presently excessively expensive, the present development and testing of LCMP sensors whose cost would not exceed 1-5 k€ give first hopes that it could become realistic in the near term (see Appendix B).

The potential for monitoring sectoral budgets could be further increased by the use of isotopic measurements such as ^{13}C and ^{14}C (Lopez et al., 2013; Vogel et al., 2013) and of co-emitted pollutants such as NO_x and CO (Ammoura et al., 2014) whose ratio to CO_2 depend on the sectors of activity.

Our inversions are shown to be highly sensitive to the types of networks that we have defined, and sometimes (e.g. for the agriculture sector) to the specific station location for given type of network. While the results could be improved if the stations location would follow some empirical rules (e.g. redistributing more stations along road networks or around power plants to better distinguish emissions from road transport and energy production), this motivates optimal network design studies, based on atmospheric inversion OSSEs such as in this study, potentially coupled to optimization algorithms (Wu and Bocquet, 2011).

One may consider further improving the current city scale inventories as a natural choice for emission accounting in the context of MRV, in a way similar to what is experienced by the applications of national inventories under UNFCCC and the Kyoto Protocol. However such refinement requires tedious efforts in order to continuously collect detailed and high-quality

1 local data. In this paper we highlight the potential of the alternative approach of atmospheric
2 inversion to provide accurate estimates of the total and sectorial budgets of the emissions.

3 Atmospheric inversion distinguishes itself in a number of ways for the quantification of city
4 CO₂ emissions. It would provide an estimate method other than inventories based on IPCC
5 guidelines. Estimating the same source of emissions with two different approaches remains
6 the best way to detect biases, even when the approaches may not be fully independent. In
7 addition to the verification of inventories, atmospheric inversion can also incorporate,
8 whenever available, inventories into its modeling framework to improve their emission
9 estimates. The inverse modeling system assimilating a cohort of measurements can provide a
10 unique platform to investigate the urban carbon cycle (e.g. the anthropogenic/biogenic land-
11 atmosphere carbon exchange of the urban ecosystem, and the carbon flows into and out of the
12 urban area) and its implication on policy-making. Finally, atmospheric inversion would bring
13 a continuous monitoring of emissions changes (e.g. larger heating emissions during cold
14 spells, and larger than usual traffic emissions during specific events) which offers important
15 possibilities for infrastructure operators to take appropriate measures with a fast response time.
16 This is in particular helpful to verify city climate mitigation actions, when their impacts could
17 be seen objectively in measured atmospheric signals. With these features, atmospheric
18 inversion appears to be a promising MRV tool to mitigate city CO₂ emissions.

Appendix A Brief review of existing city emission inventories and discussion on the accuracy of MRV city frameworks

19 Inventories of CO₂ emissions are mostly based on a calculation methodology that multiplies
20 activity data by emission factors and sums the resulting multiplications over various sectors of
21 sources. The level of source disaggregation ranges from very small (e.g. using an average
22 emission factor for all vehicles and a single traffic index for transport emissions) to very
23 detailed (e.g. using different emission factors for different vehicle types, age, driving habits,
24 traffic types, and road states). Very detailed inventories are more costly than simple ones
25 because they imply collections of larger datasets, often including specific field or laboratory
26 measurements of emission factors. This is especially true for city inventories which are driven
27 by complex socio-economic and technical factors, and can strongly vary in time and space.
28 Such complexity may question the underlying assumption of linear emission models, and
29 certainly leads to high uncertainties in both activity data and emission factors, with a typical

case being insufficient representation of source- or context-specific activities using proxy data or default/generalized emission factors. This would raise an issue of inventory verification.

The existing city inventories, in our opinion, can be roughly catalogued into three types depending on the methodology used to derive them, on their availability and on their uncertainty. The type 1 inventories are based on existing low cost frameworks. They only report at the annual and community resolution (Bertoldi et al., 2010; Cochran, 2015). Many of them adopt the 2006 IPCC Guidelines with adjustments to specific city context (City of Rio de Janeiro, 2011; Dienst et al., 2013) but without uncertainty quantification (Bellassen and Stephan, 2015); others follow the guidelines or methodologies developed by national/regional/local governments or non-profit local organizations/institutes (e.g. the Bilan Carbone methods in France (ADEME, 2010)), as well as by international organizations – such as the newly proposed GPC standard designed by C40, Local Governments for Sustainability (ICLEI) and World Resources Institute (WRI) in the support of the World Bank, UN-HABITAT and UNEP. This type of inventories can cover not only direct city emissions (i.e. the Scope 1 emissions) but also indirect or embodied emissions that are linked with cities activities but occur outside the considered territories (e.g. the Scope 2 emissions related to the consumption of purchased electricity, heat or steam; and the Scope 3 emissions related to the consumption of other products and services not covered in Scope 2; see WRI/WBCSD (2011)). In practice, the compilation of type-1 inventories can be performed with a limited cost that scales with the size of cities (e.g. ~18 k€ per year for ~1 million inhabitants excluding Scope 3 emissions (Cochran, 2015)). To date, the type-1 inventories bear high and more importantly *undocumented* uncertainties.

The type 2 inventories are those that can be derived from global or regional gridded maps of emissions estimates. They have been mainly used by the scientific community to model the atmospheric transport of CO₂. Examples are the Emissions Database for Global Atmospheric Research (EDGAR) from the European Commission Joint Research Centre (JRC) and the Netherlands Environmental Assessment Agency (<http://edgar.jrc.ec.europa.eu>), the global/regional inventory developed by the Institute of Energy Economics and the Rational Use of Energy (IER) at the University of Stuttgart (Pregger et al., 2007), and the global fossil fuel CO₂ emission map from the Peking University (PKU-CO₂; Wang et al. (2013)). The activity data and emission factors for the compilation of type-2 inventories are usually defined

1 from scales coarser than the city scale, which leads to large and, again, *undocumented*
2 uncertainty locally.

3 The type 3 inventories are compiled based upon local data down to the building/street scale at
4 the urban landscape. They are arguably more realistic than the two previous ones, but
5 available for a small number of cities to our knowledge. Examples of this type are the
6 AIRPARIF inventory for IDF (AIRPARIF, 2013), the London Atmospheric Emissions
7 Inventory (LAEI; GLA (2012)), and the inventory from the HESTIA project for Indianapolis
8 (Gurney et al., 2012). Developing a type-3 inventory is time consuming: it usually demands
9 institutional efforts and requires a high level of expertise. Type-3 inventories can only be
10 established in cities where good activity and/or fuel consumption data are accessible. The
11 inventory quality would be better if some central authority was responsible for ensuring that
12 adequate data are consistently, transparently and timely reported by public and private players
13 responsible for emissions. Uncertainty quantification for a type-3 inventory, being a difficult
14 issue due to their complexity, nevertheless can be performed in an approximate way
15 according to the expert judgment of the inventory compilers. As an example, the monthly
16 uncertainty in the Paris type-3 inventory is estimated to be of the order of 20% by the
17 AIRPARIF engineers (see Bréon et al. (2015)).

18 Both type 2 and 3 inventories mainly account for direct emissions generated within the
19 considered territories. Whatever their type (1, 2 or 3), the inventories at city scale are not
20 frequently updated because the necessary data are usually disclosed and processed long after
21 emissions actually happened. In case of revisions in calculation methods, such as the
22 correction of emission factors or the addition of emitting activities that were ignored in the
23 previous versions, the entire emission inventory has to be recomputed, which imposes a
24 traceability framework for comparing different versions. In the case of the Paris type-3
25 inventory, there is only a new update every two years with a 2-year lag between the date of
26 release and the corresponding year of emissions.

27 The IER inventory used for the practical implementation of the OSSEs in this study
28 incorporates local data to provide a gridded inventory at 1 km and 1 h resolution. We detail
29 this inventory in the main text of the paper (Sect. 2.4.1). Here we group the 40 sectors from
30 this IER inventory into seven aggregate larger sectors, and list their annual budgets in
31 Table A1.

1 The uncertainty in city emissions estimates is in general considered as larger than that in
2 national estimates (Duren and Miller, 2012). However, the development of city scale MRV
3 frameworks could foster the development of city scale inventories with an accuracy which is
4 close to that presently diagnosed for national inventories in OECD countries, reported under
5 UNFCCC and the Kyoto protocol (Chang and Bellassen, 2015). The underlying rationale is
6 that MRVs at national and city scales would have similar objectives. Both would support
7 determination of baselines and/or reduction of emissions from various sources (e.g.
8 transportation, building, and industries) for a given geographical area. As mitigation actions
9 against CO₂ emissions are many and various, their MRVs differ from one another accordingly.
10 Ninomiya (2012) classified different existing MRVs and suggested that the MRV of emission
11 reductions by actions/policies would be less accurate than the MRV of national emissions
12 using inventories. If this reasoning is also valid at the city scale, the uncertainty level for total
13 city emissions would be stringent for the MRV of emission reductions by citywide
14 actions/policies.

Appendix B Requirements on the cost of the infrastructure and of the LCMP sensors underlying the deployment and operation of dense networks

15
16 The typical cost of existing inventories give ideas on the order of magnitude which could be
17 acceptable for the cost of the overall inversion framework. Since there is presently no MRV
18 framework at the city scale, we investigate the typical cost of national inventories in the MRV
19 framework of UNFCCC. In order to have the same accuracy within the frame of MRV
20 systems, city scale inventories based on similar methodologies would have to rely on data
21 with the same level of quality. The cost of an inventory involves the collection of large
22 datasets, and the design and implementation of the inventory model. The data (e.g. statistics
23 on energy fuel consumption, transport and industrial activities) required for the development
24 of a national inventory are in general available from national agencies. For the compilation of
25 a city inventory, tracking fuel use statistics from different origins and types and for different
26 sectors might actually prove more complicated than for a state where national statistics are
27 already firmly established by governmental agencies. The CITEPA is the agency responsible
28 for preparing the French national inventory following the IPCC guidelines. The budget of the
29 activities at CITEPA related to this national inventory is about 1.5 M€ per year (République

Française, 2015). This covers not only the compilation of the fossil fuel CO₂ emissions inventory but also (1) the compilation of the inventory for other GHG gases, (2) the compilation of the inventory for GHG emissions due to land use, land use change and forestry (LULUCF), and (3) activities other than monitoring such as the reporting, archiving and annual communication to UNFCCC reviews that are imposed by the IPCC guidelines. It is therefore complicated to assess the budget of the CO₂ fossil fuel emissions inventory at CITEPA. However, it indicates that a reasonable cost for a city inversion framework should not exceed 1-2 M€ on average per year.

Current atmospheric GHG monitoring programs have significant investment and operational costs, for example the KIC Climate CarboCountCity program (<http://www.climate-kic.org/projects/carbon-emissions-from-cities/>) incurred costs of ~4 M€ for a 3 year project period, which included installation of a few monitoring stations in Paris and Rotterdam (less than 10 sites overall), as well as salaries and mobile campaigns. The typical cost of infrastructure installation for 10-site networks, if excluding the cost of the sensors, is presently of the order of 200 k€ when deploying the network if it does not require the building of dedicated towers (as assumed in our study where stations are located at 25 magl), ~180 k€ euros per year for labor charges (data QA/QC, processing and modelling), and ~5-10 k€ per year per site for maintenance and calibration. From these previous experiments one would estimate the cost of a 70 site monitoring network of the current make to about 10 M€ for a 5 year period. A strategy is required to decrease this cost if we are hoping to benefit from the demonstrated advantages of this study of operating a 30 to 70 site networks instead of a sparse 10 site network. Data hosting, processing and QA/QC costs seem fairly uncompressible and even with more advanced data processing routines, the need to hire at least one expert modeler and field technicians to maintain the network seems unavoidable. With technological development, however, one can hope that the significant contribution of sensor cost could be reduced. Ideally, this cost of the sensors should not be significant to ensure that the budgets remains of the order of 1-2 M€ on average per year (accounting for the depreciation of the initial settings and purchases over ~10 years). Today, the sensors used by the atmospheric monitoring community need to be replaced or a major repair every 5-10 years, which presents a cost of more than 500 K€ per year for a 70 site network (accounting for the depreciation of their purchase over ~7 years). Lower-cost sensors would likely be less robust (shorter life-time) which would imply that their cost need to be at least one order of magnitude smaller to be beneficial i.e. 1-5 k€.

Current LCMP prototypes tested at LSCE in the framework of on-going European innovation projects have promising results regarding their fundamental measurement precision and temporal bias structure and could cost less than 2 k€. Still, the most critical challenge will be to ensure that atmospheric monitoring networks based on such sensors can provide accurate data with a relatively (compared to the present protocols) cheap infrastructure and calibration strategy, which needs to be demonstrated in a future study.

Appendix C Trend detection under different levels of uncertainties in annual emission estimates

Supposing that the annual fossil fuel emissions from the Paris metropolitan area have a linear trend with a 25% reduction in 15 years, and that the annual emission estimates have an 5% or 10% uncertainty, we perform Monte Carlo simulations to check to what extent that the linear trend can be detected from perturbed annual emission estimates (within the given annual uncertainty) along years. The detection results are shown in Fig. C1. With 5% annual emission uncertainty, the 25% reduction of emissions in a 15-year horizon can be detected within [18%, 32%] at 95% confidence level. In contrast, with 10% and 15% annual emission uncertainty, the corresponding detection intervals are [11%, 39%] and [3%, 46%] respectively at 95% confidence level.

Acknowledgements

This study is a contribution to the project MRV Sector funded by the European Climate Knowledge and Innovation Community (Climate-KIC). Four authors (L. Wu, G. Broquet, F. Vogel and P. Ciais) work with the industrial chair BridGES supported by the Université de Versailles Saint-Quentin-en-Yvelines, the Commissariat à l'Énergie Atomique et aux Énergies Renouvelables, the Centre National de la Recherche Scientifique, Thales Alenia Space, and Veolia. We thank François-Marie Bréon for assistance.

References

- ADEME: Bilan Carbone, Entreprises - Collectivités - Territoires, Guide méthodologique, version 6.1, objectifs et principes de comptabilisation, 2010.
- AIRPARIF: Bilan des émissions de polluants atmosphériques et de gaz à effet de serre en Ile-de-France pour l'année 2010 et historique 2000/2005: Méthodologies et résultats, AIRPARIF, association de surveillance de la qualité de l'air en Ile-de-France, 2013.
- Ammoura, L., Xueref-Remy, I., Gros, V., Baudic, A., Bonsang, B., Petit, J. E., Perrussel, O., Bonnaire, N., Sciare, J., and Chevallier, F.: Atmospheric measurements of ratios between CO₂ and co-emitted species from traffic: a tunnel study in the Paris megacity, *Atmos. Chem. Phys.*, 14, 12871-12882, 10.5194/acp-14-12871-2014, 2014.
- Bellassen, V., and Stephan, N.: Accounting for Carbon: Monitoring, Reporting and Verifying Emissions in the Climate Economy, Cambridge University Press, Cambridge, UK, 2015.
- Bertoldi, P., Cayuela, D. B., Monni, S., and de Raveschoot, R. P.: Existing Methodologies and Tools for the Development and Implementation of Sustainable Energy Action Plans (SEAP), JRC Scientific and Technical Reports, Publication number: JRC 56513, EUR 24309 EN, European Commission Joint Research Centre Institute for Energy, 2010.
- BIS: Low Carbon Environmental Goods and Services: Report for 2011/12, United Kingdom Department for Business, Innovation, and Skills (BIS), 2013.
- Boden, T. A., Marland, G., and Andres, R. J.: Global, Regional, and National Fossil-Fuel CO₂ Emissions, Carbon Dioxide Information Analysis Center, Oak Ridge National Laboratory, U.S. Department of Energy, Oak Ridge, Tenn., U.S.A., 2013.
- Bousquet, P., Peylin, P., Ciais, P., Le Quéré, C., Friedlingstein, P., and Tans, P. P.: Regional Changes in Carbon Dioxide Fluxes of Land and Oceans Since 1980, *Science*, 290, 1342-1346, 10.1126/science.290.5495.1342, 2000.
- Boussetta, S., Balsamo, G., Beljaars, A., Panareda, A.-A., Calvet, J.-C., Jacobs, C., van den Hurk, B., Viterbo, P., Lafont, S., Dutra, E., Jarlan, L., Balzarolo, M., Papale, D., and van der Werf, G.: Natural land carbon dioxide exchanges in the ECMWF integrated forecasting system: Implementation and offline validation, *J. Geophys. Res.*, 118, 5923-5946, 10.1002/jgrd.50488, 2013.
- Bréon, F. M., Broquet, G., Puygrenier, V., Chevallier, F., Xueref-Remy, I., Ramonet, M., Dieudonné, E., Lopez, M., Schmidt, M., Perrussel, O., and Ciais, P.: An attempt at estimating Paris area CO₂ emissions from atmospheric concentration measurements, *Atmos. Chem. Phys.*, 15, 1707-1724, 10.5194/acp-15-1707-2015, 2015.
- Broquet, G., Chevallier, F., Bréon, F. M., Kadygrov, N., Alemanno, M., Apadula, F., Hammer, S., Haszpra, L., Meinhardt, F., Morguí, J. A., Necki, J., Piacentino, S., Ramonet, M., Schmidt, M., Thompson, R. L., Vermeulen, A. T., Yver, C., and Ciais, P.: Regional inversion of CO₂ ecosystem fluxes from atmospheric measurements: reliability of the uncertainty estimates, *Atmos. Chem. Phys.*, 13, 9039-9056, 10.5194/acp-13-9039-2013, 2013.
- Chang, J.-P., and Bellassen, V.: Trend setter for territorial schemes: national greenhouse gas inventories under the UNFCCC, in: Accounting for Carbon: Monitoring, Reporting and Verifying Emissions in the Climate Economy, edited by: Bellassen, V., and N., S., Cambridge University Press, Cambridge, UK, 2015.

1 Chevallier, F., Impact of correlated observation errors on inverted CO₂ surface fluxes from
2 OCO measurements, *Geophys. Res. Lett.*, 34, L24804, doi:10.1029/2007GL030463, 2007.

3 Chevallier, F., Ciais, P., Conway, T. J., Aalto, T., Anderson, B. E., Bousquet, P., Brunke, E.
4 G., Ciattaglia, L., Esaki, Y., Fröhlich, M., Gomez, A., Gomez-Pelaez, A. J., Haszpra, L.,
5 Krummel, P. B., Langenfelds, R. L., Leuenberger, M., Machida, T., Maignan, F., Matsueda,
6 H., Morguí, J. A., Mukai, H., Nakazawa, T., Peylin, P., Ramonet, M., Rivier, L., Sawa, Y.,
7 Schmidt, M., Steele, L. P., Vay, S. A., Vermeulen, A. T., Wofsy, S., and Worthy, D.: CO₂
8 surface fluxes at grid point scale estimated from a global 21 year reanalysis of atmospheric
9 measurements, *J. Geophys. Res.*, 115, D21307, 10.1029/2010jd013887, 2010.

10 Ciais, P., Sabine, C., Bala, G., Bopp, L., Brovkin, V., Canadell, J., Chhabra, A., DeFries, R.,
11 Galloway, J., Heimann, M., C.Jones, Quéré, C. L., Myneni, R. B., Piao, S., and Thornton, P.:
12 Carbon and Other Biogeochemical Cycles, *Climate Change 2013: The Physical Science*
13 *Basis. Contribution of Working Group I to the Fifth Assessment Report of the*
14 *Intergovernmental Panel on Climate Change*, Cambridge University Press, 2013.

15 CITEPA: Inventaire des émissions de polluants atmosphériques et de gaz à effet de serre en
16 France, Format SECTEN, 2014.

17 City of Rio de Janeiro: Greenhouse Gas Inventory and Emissions Scenario of Rio de Janeiro,
18 Brazil: Technical Summary, COPPE/UFRJ and Rio Prefeitura, 2011.

19 Clapp, C., Leseur, A., Sartor, O., Briner, G., and Corfee-Morlot, J.: Cities and Carbon Market
20 Finance: Taking Stock of Cities' Experience With Clean Development Mechanism (CDM)
21 and Joint Implementation (JI), 2010.

22 Cochran, I.: Region/City Geographical Inventorie, in: *Accounting for Carbon: Monitoring,*
23 *Reporting and Verifying Emissions in the Climate Economy*, edited by: Bellassen, V., and N.,
24 S., Cambridge University Press, Cambridge, UK, 2015.

25 Couvidat, F., Kim, Y., Sartelet, K., Seigneur, C., Marchand, N., and Sciare, J.: Modeling
26 secondary organic aerosol in an urban area: application to Paris, France, *Atmos. Chem. Phys.*,
27 13, 983-996, 10.5194/acp-13-983-2013, 2013.

28 Dienst, C., Schneider, C., Xia, C., Saurat, M., Fischer, T., and Vallentin, D.: On Track to
29 Become a Low Carbon Future City? First Findings of the Integrated Status Quo and Trends
30 Assessment of the Pilot City of Wuxi in China, *Sustainability*, 5, 3224-3243, 2013.

31 Duren, R. M., and Miller, C. E.: Measuring the carbon emissions of megacities, *Nature Clim.*
32 *Change*, 2, 560-562, 2012.

33 Enting, I.: *Inverse Problems in Atmospheric Constituent Transport*, Cambridge University
34 Press, Cambridge, United Kingdom, 2002.

35 Erickson, P., and Tempest, K.: *Advancing climate ambition: Cities as partners in global*
36 *climate action*, Produced by Stockholm Environment Institute (SEI) in support of the UN
37 Secretary-General's Special Envoy for Cities and Climate Change and C40, 2014.

38 Fauser, P., Sørensen, P. B., Nielsen, M., Winther, M., Plejdrup, M. S., Hoffmann, L.,
39 Gyldenkerne, S., Mikkelsen, M. H., Albrektsen, R., Lyck, E., Thomsen, M., Hjelgaard, K.,
40 and Nielsen, O.-K.: Monte Carlo (Tier 2) uncertainty analysis of Danish Greenhouse gas
41 emission inventory, *Greenhouse Gas Measurement and Management*, 1, 145-160,
42 10.1080/20430779.2011.621949, 2011.

43 Fong, W. K., Sotos, M., Doust, M., Schultz, S., Marques, A., Deng-Beck, C., and coauthors:
44 *Global Protocol for Community-Scale Greenhouse Gas Emission Inventories - An*

1 Accounting and Reporting Standard for Cities, World Resources Institute, C40 Cities Climate
2 Leadership Group and Local Governments for Sustainability (ICLEI), 2014.

3 République Française, État récapitulatif de l'effort financier consenti en 2014 et prévu en 2015
4 au titre de la protection de la nature et de l'environnement, Annexe au projet de loi de finances
5 pour 2015, Budget. 2015 (Fascicules jaunes), Direction générale des finances publiques,
6 2015.

7 GLA: London Atmospheric Emissions Inventory 2010, Greater London Authority, 2012.

8 Glaeser, E. L. and Kahn, M. E., The greenness of cities: Carbon dioxide emissions and urban
9 development, *J. Urban Econ.*, 67, 404–418, 2010

10 Gurney, K. R., Law, R. M., Denning, A. S., Rayner, P. J., Baker, D., Bousquet, P., Bruhwiler,
11 L., Chen, Y.-H., Ciais, P., Fan, S., Fung, I. Y., Gloor, M., Heimann, M., Higuchi, K., John, J.,
12 Maki, T., Maksyutov, S., Masarie, K., Peylin, P., Prather, M., Pak, B. C., Randerson, J.,
13 Sarmiento, J., Taguchi, S., Takahashi, T., and Yuen, C.-W.: Towards robust regional
14 estimates of CO₂ sources and sinks using atmospheric transport models, *Nature*, 415, 626-
15 630, 2002.

16 Gurney, K. R., Razlivanov, I., Song, Y., Zhou, Y., Benes, B., and Abdul-Massih, M.:
17 Quantification of Fossil Fuel CO₂ Emissions on the Building/Street Scale for a Large U.S.
18 City, *Environ. Sci. Technol.*, 46, 12194-12202, 10.1021/es3011282, 2012.

19 Howard, A.: FVA, NMA and NMM technical papers, Lima, Peru, 2014.

20 Hutyra, L. R., Duren, R., Gurney, K. R., Grimm, N., Kort, E. A., Larson, E., and Shrestha, G.:
21 Urbanization and the carbon cycle: Current capabilities and research outlook from the natural
22 sciences perspective, *Earth's Future*, 2, 2014EF000255, 10.1002/2014ef000255, 2014.

23 IEA: World energy outlook, International Energy Agency (IEA), Paris, 2008.

24 IGES: Measurement, Reporting and Verification (MRV) for low carbon development:
25 Learning from experience in Asia, IGES Policy Report No. 2012-03, Institute for Global
26 Environmental Strategies (IGES), Kanagawa, Japan, 2012.

27 Kort, E. A., Angevine, W. M., Duren, R., and Miller, C. E.: Surface observations for
28 monitoring urban fossil fuel CO₂ emissions: Minimum site location requirements for the Los
29 Angeles megacity, *J. Geophys. Res.*, 118, 1577-1584, 10.1002/jgrd.50135, 2013.

30 Latoska, A.: Erstellung eines räumlich hoch aufgelösten Emissionsinventar von
31 Luftschadstoffen am Beispiel von Erstellung eines räumlich hoch aufgelösten, Thesis, Institut
32 für Energiewirtschaft und Rationelle Energieanwendung, Universität Stuttgart, 2009.

33 Lauvaux, T., Miles, N. L., Richardson, S. J., Deng, A., Stauffer, D. R., Davis, K. J., Jacobson,
34 G., Rella, C., Calonder, G.-P., and DeCola, P. L.: Urban Emissions of CO₂ from Davos,
35 Switzerland: The First Real-Time Monitoring System Using an Atmospheric Inversion
36 Technique, *J. Appl. Meteor. Climatol.*, 52, 2654-2668, 10.1175/jamc-d-13-038.1, 2013.

37 Liu, Z., He, C., Zhou, Y., and Wu, J.: How much of the world's land has been urbanized,
38 really? A hierarchical framework for avoiding confusion, *Landscape Ecol.*, 29, 763-771,
39 10.1007/s10980-014-0034-y, 2014.

40 Lopez, M., Schmidt, M., Delmotte, M., Colomb, A., Gros, V., Janssen, C., Lehman, S. J.,
41 Mondelain, D., Perrussel, O., Ramonet, M., Xueref-Remy, I., and Bousquet, P.: CO, NO_x and
42 ¹³CO₂ as tracers for fossil fuel CO₂: results from a pilot study in Paris during winter 2010,
43 *Atmos. Chem. Phys.*, 13, 7343-7358, 10.5194/acp-13-7343-2013, 2013.

1 Mairie de Paris: BLEU Climat 2012, l'engagement de la collectivité parisienne en matière de
2 lutte contre les émissions de gas à effet de serre et d'efficacité énergétique, 2012.

3 Marr, M. A., and Wehner, S.: Cities and Carbon Finance: a Feasibility Study on an Urban
4 CDM, UNEP (United Nations Environment Programme) / Gwangju City, 2012.

5 McKain, K., Wofsy, S. C., Nehrkorn, T., Eluszkiewicz, J., Ehleringer, J. R., and Stephens, B.
6 B.: Assessment of ground-based atmospheric observations for verification of greenhouse gas
7 emissions from an urban region, *Proceedings of the National Academy of Sciences*, 109,
8 8423-8428, 10.1073/pnas.1116645109, 2012.

9 Meinshausen, M., Meinshausen, N., Hare, W., Raper, S. C. B., Frieler, K., Knutti, R., Frame,
10 D. J., and Allen, M. R.: Greenhouse-gas emission targets for limiting global warming to 2°C,
11 *Nature*, 458, 1158-1162, 2009.

12 Menut, L., Bessagnet, B., Khvorostyanov, D., Beekmann, M., Blond, N., Colette, A., Coll, I.,
13 Curci, G., Foret, G., Hodzic, A., Mailler, S., Meleux, F., Monge, J. L., Pison, I., Siour, G.,
14 Turquety, S., Valari, M., Vautard, R., and Vivanco, M. G.: CHIMERE 2013: a model for
15 regional atmospheric composition modelling, *Geosci. Model Dev.*, 6, 981-1028,
16 10.5194/gmd-6-981-2013, 2013.

17 Ninomiya, Y.: Classification of MRV of Greenhouse Gas (GHG) Emissions/Reductions: For
18 the discussions on NAMAs and MRV, Institute for Global Environmental Strategies (IGES),
19 2012.

20 Nordbo, A., Järvi, L., Haapanala, S., Wood, C. R., and Vesala, T.: Fraction of natural area as
21 main predictor of net CO₂ emissions from cities, *Geophys. Res. Lett.*, 39, L20802,
22 10.1029/2012gl053087, 2012.

23 Pacala, S., Breidenich, C., Brewer, P. G., Fung, I., Gunson, M. R., Heddle, G., Law, B.,
24 Marland, G., Paustian, K., and Prather, K.: Verifying Greenhouse Gas Emissions: Methods to
25 Support International Climate Agreements, The National Academies Press, Washington, DC,
26 124 pp., 2010.

27 Pataki, D. E., Bowling, D. R., and Ehleringer, J. R.: Seasonal cycle of carbon dioxide and its
28 isotopic composition in an urban atmosphere: Anthropogenic and biogenic effects, *J.*
29 *Geophys. Res.*, 108, D23, 4735, doi:4710.1029/2003JD003865, 2003

30 Peters, W., Jacobson, A. R., Sweeney, C., Andrews, A. E., Conway, T. J., Masarie, K., Miller,
31 J. B., Bruhwiler, L. M. P., Pétron, G., Hirsch, A. I., Worthy, D. E. J., van der Werf, G. R.,
32 Randerson, J. T., Wennberg, P. O., Krol, M. C., and Tans, P. P.: An atmospheric perspective
33 on North American carbon dioxide exchange: CarbonTracker, *Proceedings of the National*
34 *Academy of Sciences*, 104, 18925-18930, 10.1073/pnas.0708986104, 2007.

35 Pregger, T., Scholz, Y., and Friedrich, R.: Documentation of the Anthropogenic GHG
36 Emission Data for Europe Provided in the Frame of CarboEurope GHG and CarboEurope IP,
37 Final Report CarboEurope-IP, Institute for Energy Economics and the Rational Use of Energy
38 (IER), University of Stuttgart, Stuttgart, Germany, 2007.

39 Reckien, D., Flacke, J., Dawson, R. J., Heidrich, O., Olazabal, M., Foley, A., Hamann, J. J. P.,
40 Orru, H., Salvia, M., De Gregorio Hurtado, S., Geneletti, D., and Pietrapertosa, F.: Climate
41 change response in Europe: what's the reality? Analysis of adaptation and mitigation plans
42 from 200 urban areas in 11 countries, *Clim. Chang.*, 122, 331-340, 10.1007/s10584-013-
43 0989-8, 2013.

1 Rodgers, C. D.: Inverse Methods for Atmospheric Sounding: Theory and Practice, Series on
2 Atmospheric, Oceanic and Planetary Physics, edited by: Taylor, F. W., World Scientific,
3 2000.

4 Rosenzweig, C., Solecki, W., Hammer, S. A., and Mehrotra, S.: Cities lead the way in
5 climate-change action, *Nature*, 467, 909-911, 2010.

6 Seibert, P., Beyrich, F., Gryning, S.-E., Joffre, S., Rasmussen, A., and Tercier, P.: Review and
7 intercomparison of operational methods for the determination of the mixing height, *Atmos.*
8 *Environ.*, 34, 1001-1027, [http://dx.doi.org/10.1016/S1352-2310\(99\)00349-0](http://dx.doi.org/10.1016/S1352-2310(99)00349-0), 2000.

9 Seto, K. C., Dhakal, S., Bigio, A., Blanco, H., Delgado, G. C., Dewar, D., Huang, L., Inaba,
10 A., Kansal, A., Lwasa, S., McMahon, J. E., Müller, D. B., Murakami, J., Nagendra, H., and
11 Ramaswami, A.: Human settlements, infrastructure and spatial planning, in: *Climate Change*
12 *2014: Mitigation of Climate Change. Contribution of Working Group III to the Fifth*
13 *Assessment Report of the Intergovernmental Panel on Climate Change*, edited by: Edenhofer,
14 O., Pichs-Madruga, R., Sokona, Y., Farahani, E., Kadner, S., Seyboth, K., Adler, A., Baum,
15 I., Brunner, S., Eickemeier, P., Kriemann, B., Savolainen, J., Schlömer, S., von Stechow, C.,
16 Zwickel, T., and Minx, J. C., Cambridge, United Kingdom and New York, NY, USA, 2014.

17 Shah, N., Vallejo, L., Cockerill, T., Gambhir, A., Heyes, A., Hills, T., Jennings, M., Jones, O.,
18 Kalas, N., Keirstead, J., Khor, C., Mazur, C., Napp, T., Strapasson, A., Tong, D., and Woods,
19 J.: Halving global CO₂ by 2050: technologies and costs, *Energy Futures Lab and Grantham*
20 *Institute for Climate Change at Imperial College London*, 2013.

21 Staufer, J., Broquet, G., Bréon, F.-M., Puygrenier, V., Chevallier, F., Xueref-Rémy, Elsa
22 Dieudonné, E., Lopez, M., Schmidt, M., Ramonet, M., Perrussel, O., Lac, C., Wu, L., and
23 Ciais, P.: A first year-long estimate of the Paris region anthropogenic CO₂ emissions based
24 on atmospheric inversion, *Atmos. Chem. Phys. Discuss.*, doi:10.5194/acp-2016-191, 2016.

25 Steeneveld, G. J., Vilà-Guerau de Arellano, J., Holtslag, A. A. M., Mauritsen, T., Svensson,
26 G., and de Bruijn, E. I. F.: Evaluation of Limited-Area Models for the Representation of the
27 Diurnal Cycle and Contrasting Nights in CASES-99, *J. Appl. Meteor. Climatol.*, 47, 869-887,
28 10.1175/2007jamc1702.1, 2008.

29 Sugar, L., and Kennedy, C.: A low carbon infrastructure plan for Toronto, Canada, *Can. J.*
30 *Civ. Eng.*, 40, 86-96, doi:10.1139/cjce-2011-0523, 2013.

31 The Gold Standard: Financing cities of the future: Tools to scale-up clean urban development,
32 2014.

33 TMG: Tokyo Cap-and-Trade Program - Japan's First Mandatory Emissions Trading Scheme,
34 TMG, Tokyo, 2010.

35 UN: World Urbanization Prospects: The 2014 Revision, HighlightsST/ESA/SER.A/352,
36 2014.

37 UNEP: The Emissions Gap Report 2013, United Nations Environment Programme (UNEP),
38 Nairobi, 2013.

39 UNEP: Climate Finance for Cities and Buildings - A Handbook for Local Governments,
40 UNEP Division of Technology, Industry and Economics (DTIE), Paris, 2014.

41 UNFCCC: Establishment of an Ad Hoc Working Group on the Durban Platform for
42 Enhanced Action, Decision 1/CP.17, FCCC/CP/2011/9/Add.1, 2011.

1 Vogel, F. R., Tiruchittampalam, B., Theloke, J., Kretschmer, R., Gerbig, C., Hammer, S., and
2 Levin, I.: Can we evaluate a fine-grained emission model using high-resolution atmospheric
3 transport modelling and regional fossil fuel CO₂ observations? *Tellus B*, 65, 18681, 2013.

4 Wang-Helmreich, H., Kreibich, N., Streitferdt, V., Arens, C., and Sterk, W.: City-Wide
5 Programmes of Activities - An Option for Significant Emission Reductions in Cities? JIKO
6 Policy Paper 04/2012, Wuppertal Institute for Climate, Environment and Energy, 2012.

7 Wang, R., Tao, S., Ciais, P., Shen, H. Z., Huang, Y., Chen, H., Shen, G. F., Wang, B., Li, W.,
8 Zhang, Y. Y., Lu, Y., Zhu, D., Chen, Y. C., Liu, X. P., Wang, W. T., Wang, X. L., Liu, W.
9 X., Li, B. G., and Piao, S. L.: High-resolution mapping of combustion processes and
10 implications for CO₂ emissions, *Atmos. Chem. Phys.*, 13, 5189-5203, 10.5194/acp-13-5189-
11 2013, 2013.

12 World Bank: A city-wide approach to carbon finance, Carbon Partnership Facility Innovation
13 Series, Washington, DC, 2010.

14 WRI/WBCSD: The Greenhouse Gas Protocol: A Corporate Accounting and Reporting
15 Standard, World Resources Institute/World Business Council on Sustainable Development,
16 Washington, D. C., 2011.

17 Wu, L., and Bocquet, M.: Optimal redistribution of the background ozone monitoring stations
18 over France, *Atmos. Environ.*, 45, 772-783,
19 <http://dx.doi.org/10.1016/j.atmosenv.2010.08.038>, 2011.

20 Wu, L., Bocquet, M., Lauvaux, T., Chevallier, F., Rayner, P., and Davis, K.: Optimal
21 representation of source-sink fluxes for mesoscale carbon dioxide inversion with synthetic
22 data, *J. Geophys. Res.*, 116, D21304, 10.1029/2011jd016198, 2011.

23 Zhang, Q. J., Beekmann, M., Drewnick, F., Freutel, F., Schneider, J., Crippa, M., Prevot, A.
24 S. H., Baltensperger, U., Poulain, L., Wiedensohler, A., Sciare, J., Gros, V., Borbon, A.,
25 Colomb, A., Michoud, V., Doussin, J. F., Denier van der Gon, H. A. C., Haeffelin, M.,
26 Dupont, J. C., Siour, G., Petetin, H., Bessagnet, B., Pandis, S. N., Hodzic, A., Sanchez, O.,
27 Honoré, C., and Perrussel, O.: Formation of organic aerosol in the Paris region during the
28 MEGAPOLI summer campaign: evaluation of the volatility-basis-set approach within the
29 CHIMERE model, *Atmos. Chem. Phys.*, 13, 5767-5790, 10.5194/acp-13-5767-2013, 2013.
30

Table 1 Spatiotemporal resolutions of the sectoral control factors for inversions over 30-day periods (see the main text and Table A1 for more information on aggregate sectors).

Control factors	Spatial resolution	Time resolution	Number of factors
Building	5 zone	Daily daytime and night-time	300
Road	5 zones	Daily daytime and night-time	300
Energy	1 zone	Daily daytime and night-time	60
Production	1 zone	Daily daytime and night-time	60
Agriculture	1 zone	Daily	30
Airline	1 zone	Daily	30
Rest	1 zone	Daily	30
NEE	1 zone	5-day period with four daily 6h-windows	24
--	--	--	834 (total)

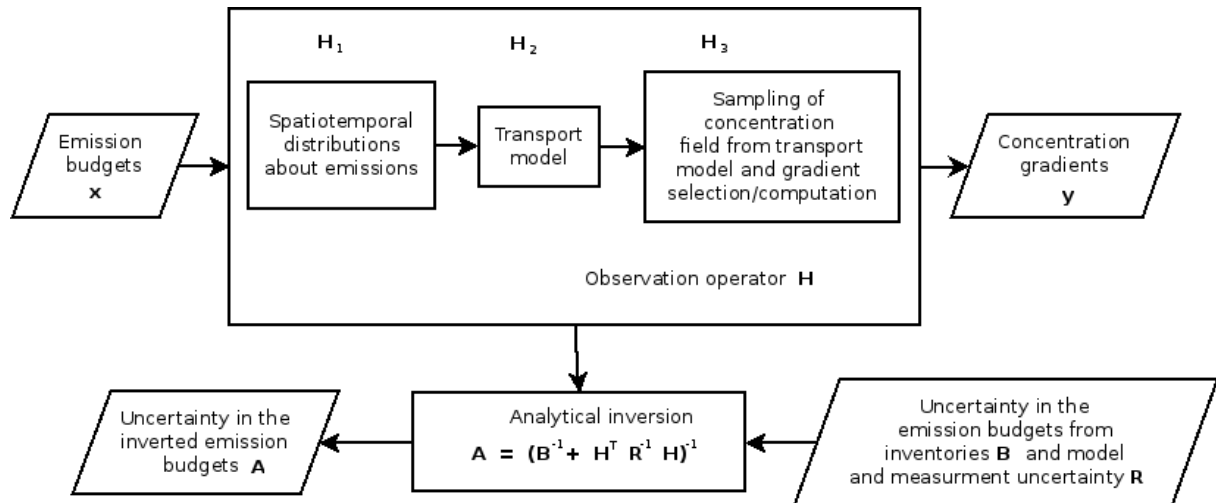
44

- 1 Table A1 Specification of the 40 sectors in the IER inventory employed in this study. These
2 sectors are grouped into seven aggregate larger sectors listed in Table 1.

Sector	NFR code	Budget (TgC/yr)	Comments
Energy	1A1a	3.7205	Public Electricity and Heat Production
	1A1b	0.31007	Petroleum Refining
	1A1c	0.097906	Manufacture of Solid Fuels and Other Energy Industries
Road	1A3bi	3.0287	Passenger cars
	1A3biii	0.78072	Heavy duty vehicles
	1A3bii	0.66808	Light duty vehicles
Building	1A4bi	2.5757	Residential plants
	1A4ai	1.0185	Commercial / Institutional
	1A4bii	0.90577	Household and gardening (mobile)
	1A4aii	0.4489	Commercial / Institutional
Production	1A2fi	1.0724	Fuel Combustion Activities: Manufacturing Industries and Construction
	1A2c	0.37312	Chemicals
	2A1	0.11867	Mineral Products
	1A2e	0.11245	Food Processing, Beverages & Tobacco
	1A2a	0.09999	Iron and Steel
	1A2d	0.088409	Pulp, Paper and Print
Agriculture	1A4ci	0.32116	Plants in agriculture, forestry and aquaculture
	1A4cii	0.14497	Off-road Vehicles and Other Machinery
Airline	1A3ai(i)	0.58194	International Aviation
	1A3aii(i)	0.34983	Civil Aviation (Domestic)
Rest	2B1	0.075718	Ammonia Production

6Cb	0.042929	Waste Incineration
3A2	0.038744	Paint Application
1A3biv	0.037411	Automobile tyre and brake wear
1A3e	0.031093	Other Transportation
2C1	0.020038	Metal Production
1A3c	0.019035	Railways
2A7d	0.011561	Mineral Products
2A4	0.0082194	Mineral Products
2B5a	0.0075701	Chemical Industry
3C	0.0056263	Chemical Products, Manufacture and Processing
2A3	0.0054513	Mineral Products
1A2b	0.00506	Non-ferrous Metals
2A2	0.0049208	Mineral Products
2C3	0.0044444	Metal Production
1A3dii	0.0039965	Navigation
2C2	0.0024742	Metal Production
3B1	0.0017747	Degreasing and Dry Cleaning
1B1b	0.00018562	Fugitive Emissions from Fuels
2B3	0.00013253	Chemical Industry

1



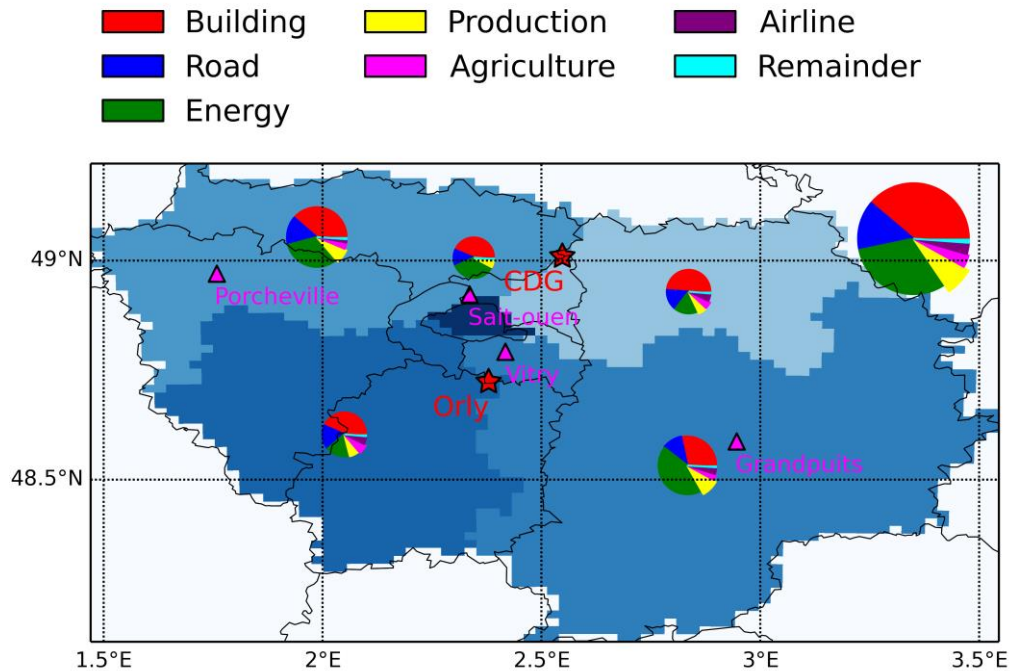
2

3

4 Fig. 1 Diagram of the principle of the city CO₂ emissions inversion system and of the
 5 computation of uncertainties in the inverted emission budgets. Note that there is no
 6 computation of \mathbf{x} and \mathbf{y} vectors in this OSSE study.

7

1
2

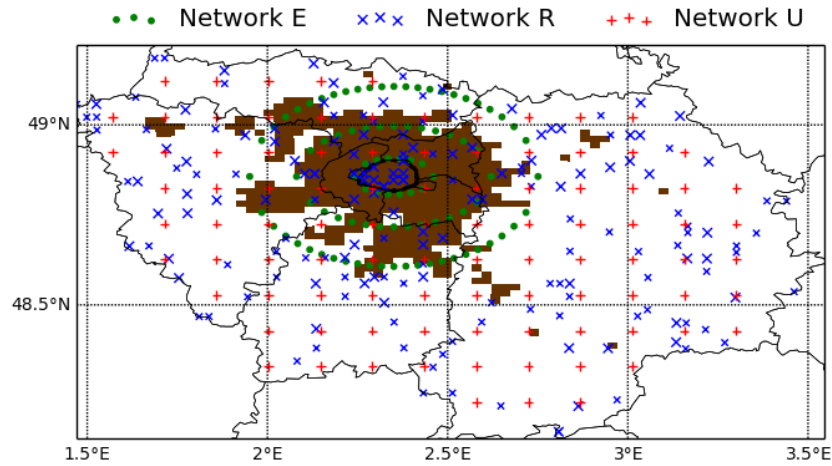


3

4 Fig. 2 Sectoral budgets of fossil fuel CO₂ emissions from the IER inventory for the five
5 “control” zones (central Paris in dark blue and four other surrounding areas in light blue)
6 partitioning the IDF region and for the month of January in 2011 (see the first seven rows in
7 Table 1 for sector specifications). The circle area is proportional to the emission budge. The
8 upper right largest circle shows the total sectoral budgets for all the five areas of IDF. The red
9 pentagons shows the two airports CDG and Orly, and the purple triangles show several large
10 point emissions such as three EDF power plants and the TOTAL Grandpuits refinery. Note
11 that these five zones in blue mark out the IDF region, but do not strictly follow the
12 administrative borders (black lines) within IDF.

13

1

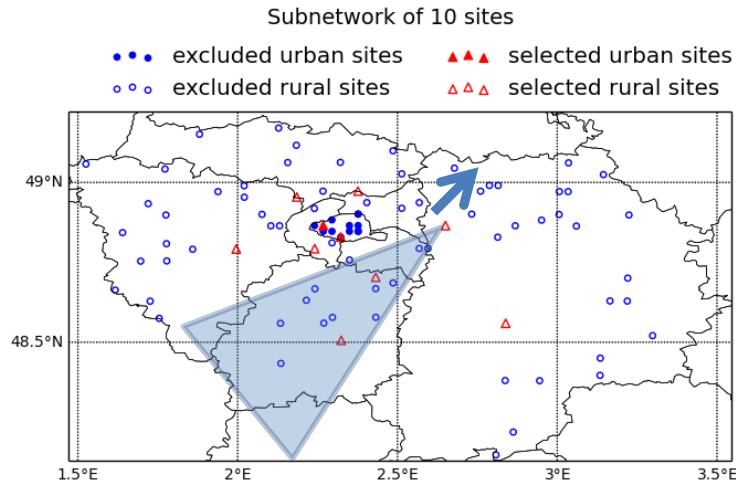


2

3 Fig. 3 Locations for the elliptical (E), random-even (R) and uniform (U) networks over IDF.
 4 The brown area marks out where the population density is larger than 1250 people per km².
 5 The E network (green dots) consists of three rings surrounding the densely populated urban
 6 area in brown. The U network (red crosses) extends to the regular grid points of the IDF
 7 domain. The site locations of the R network are randomly selected respectively in three
 8 concentric areas: (1) the city center (the administrative “city of Paris”) within the peripheral
 9 ring (coinciding with the smallest green ring), (2) the suburban area (in brown) with central
 10 Paris clipped out, and (3) the rest of IDF.

11

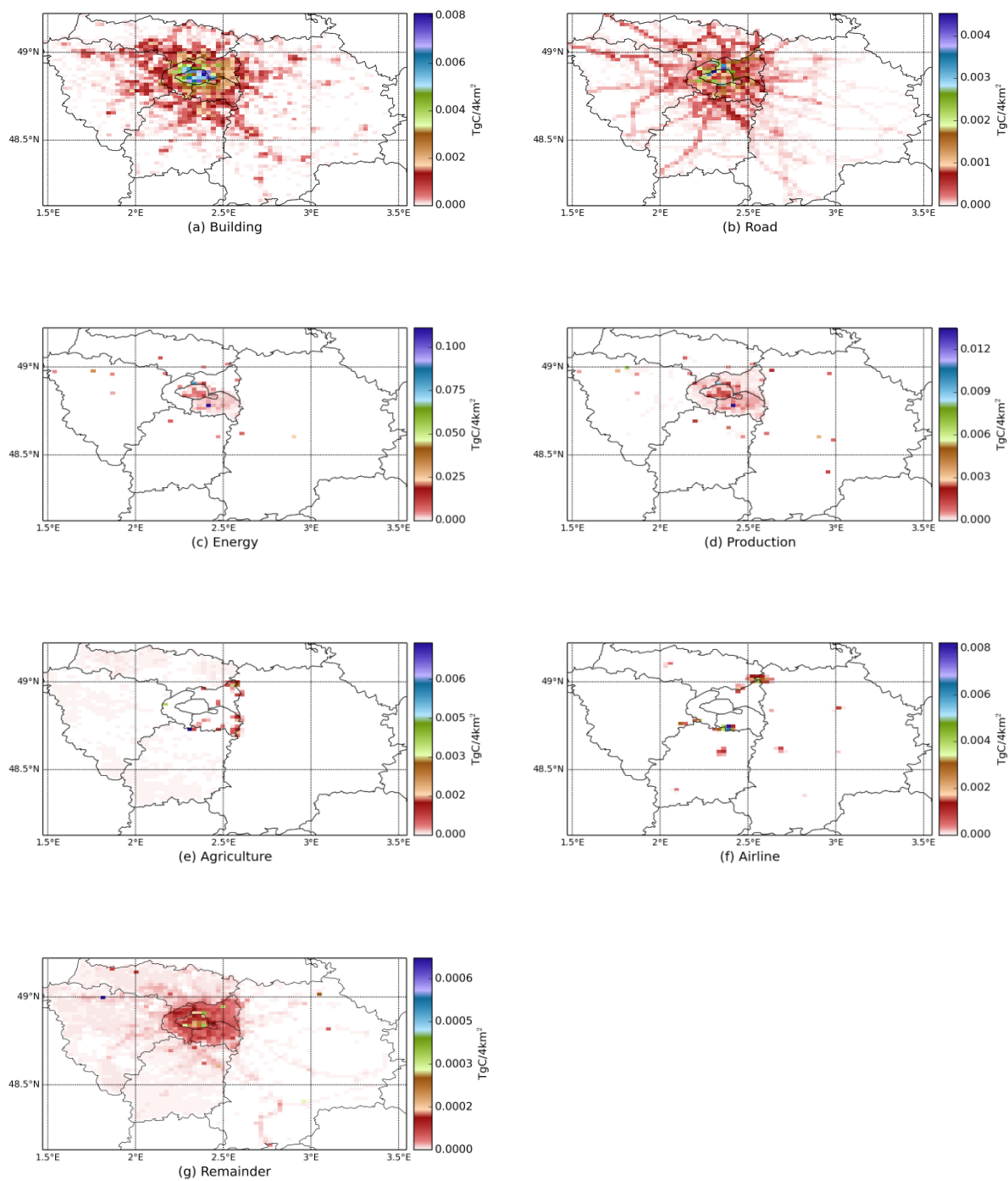
1



2

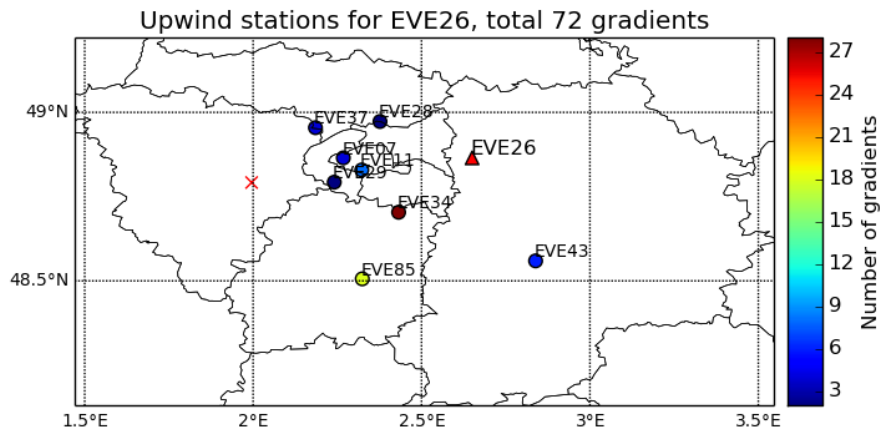
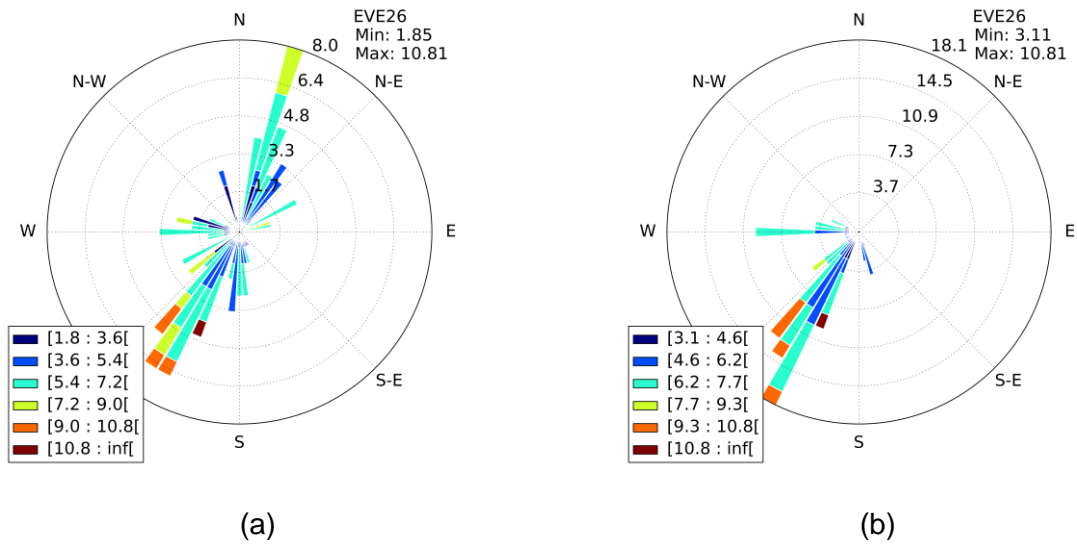
3 Fig. 4 Selection of a subset of 10 sites (red triangles) from a cloud of candidate locations for
 4 the R network to form smaller networks. The blue circles show the sites that are not selected
 5 from available locations. The open circles/triangles present rural sites, and the filled
 6 circles/triangles present urban sites. This figure also shows how the wind direction selects
 7 candidates of upwind sites for concentration gradient computations at a downwind station.
 8 The blue arrow indicates the wind direction at that downwind station. The two red triangles
 9 covered in the shadow area are candidate upwind sites according to the selection procedure
 10 detailed in Sect. 2.4.3.

11



2 Fig. 5 Sectoral and spatial distribution of the IER inventory over IDF for January 2011.

1



(c)

2 Fig. 6 Results of selections of upwind stations for gradient computations for EVE26 (see Fig.
 3 4; R-type network of 10 stations) for the month of January 2011. (a) The afternoon wind
 4 conditions at EVE26 during the given month; (b) the afternoon wind conditions for the
 5 observations selected for gradient calculation at EVE26; (c) the number of times a site is
 6 selected as upwind for gradient computations at EVE26. The leftmost red cross indicates a
 7 site that is never selected for gradient computation for EVE26.

8

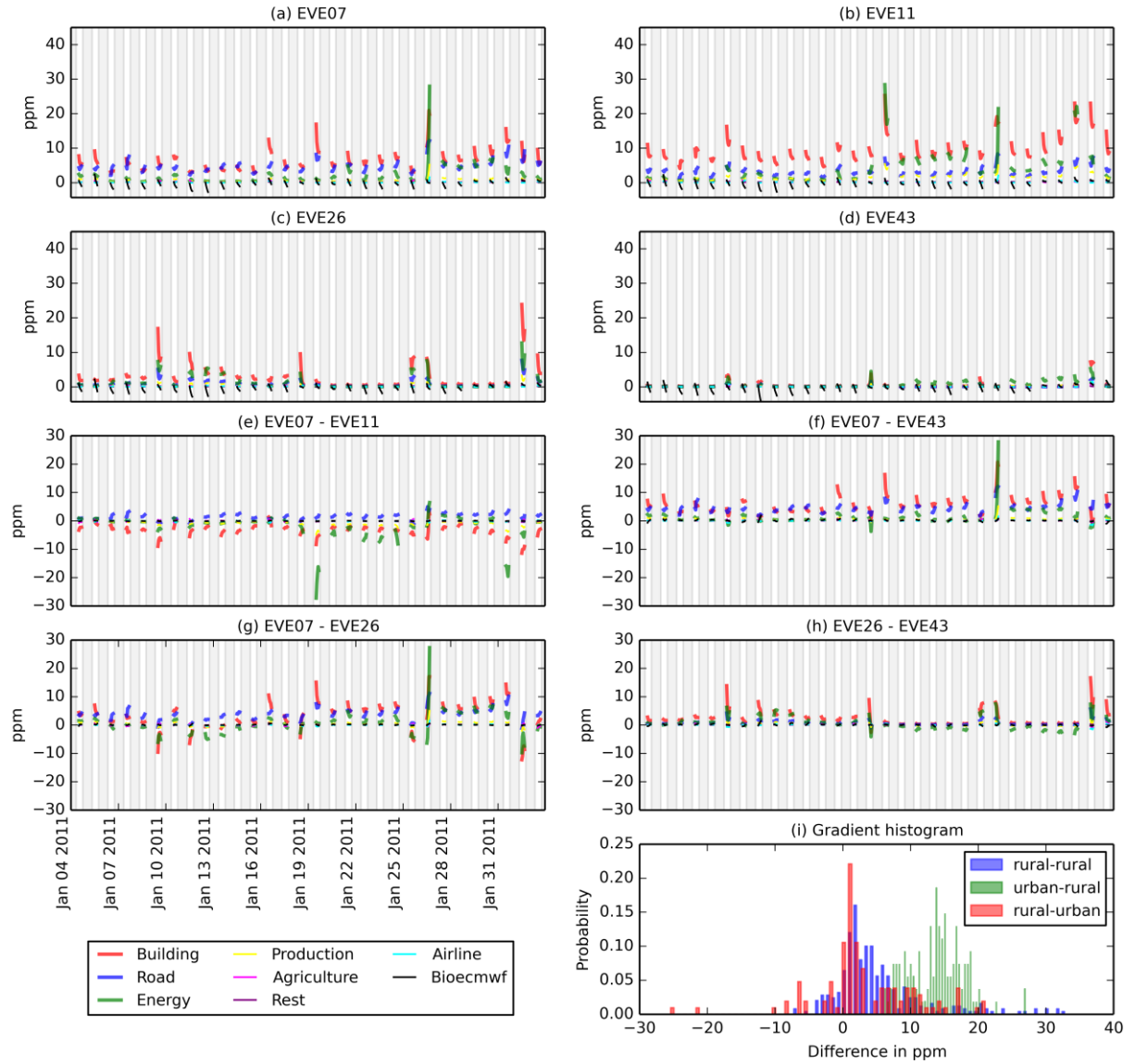
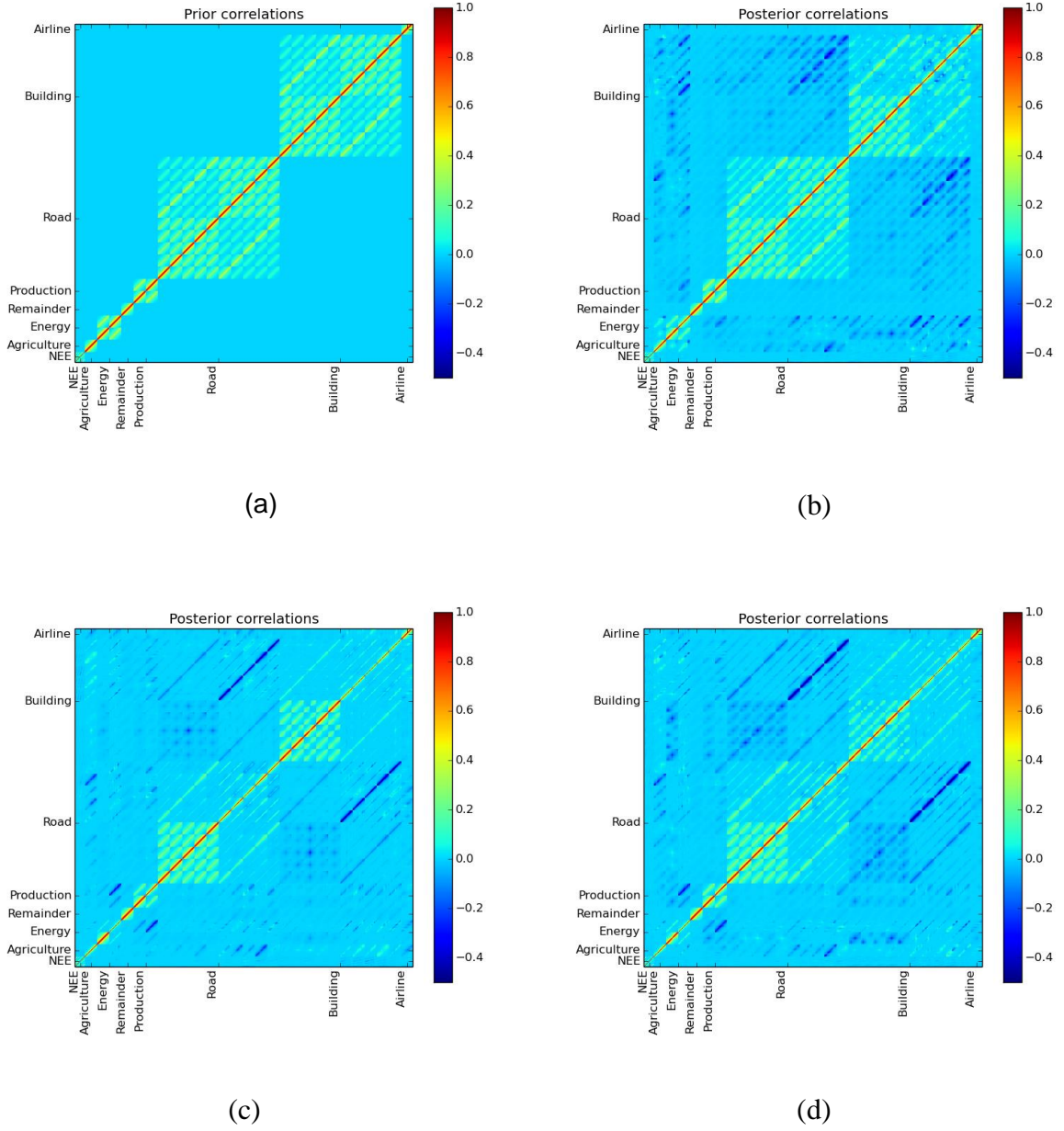
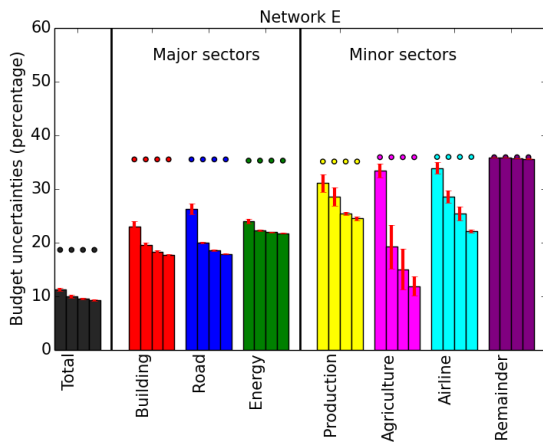


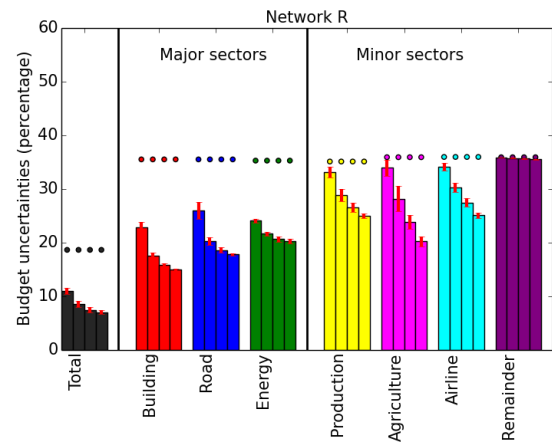
Fig. 7 (a-d) CO₂ mixing ratio series of sectoral CHIMERE simulations at four selected stations of the R network (see Fig. 4 and Fig. 6c). EVE07 and EVE11 are urban sites and EVE26 and EVE43 are rural sites but close to large point emissions. The shadow marks out the night time. (e-h) The time series of the difference in model simulations sampled at several site pairs among the four sites. (i) The histogram of afternoon concentration gradients following the data selection procedure detailed in Sect. 2.4.3 for all the 10 stations of the R network. These histograms are grouped according to the type of downwind and upwind stations.



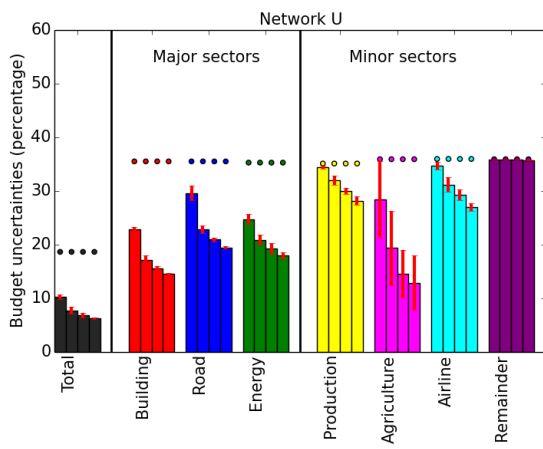
2 Fig. 8 The correlation structures in (a) the error of prior scaling factor estimates; (b) the
 3 posterior error obtained by inversion using a U network with 10 stations; (c) the posterior
 4 error obtained by inversion using an E network with 70 stations; and (d) the posterior error
 5 obtained by inversion using a U network with 70 stations. Each row or column of the pixels
 6 corresponds to the correlation between one scaling factor and all the 834 scaling factors (see
 7 Sect. 2.2). For clarity, we group these scaling factors into eight sectors and organize them for
 8 each sector according to temporal indices and spatial areas. The tickers show the name of
 9 these eight sectors.



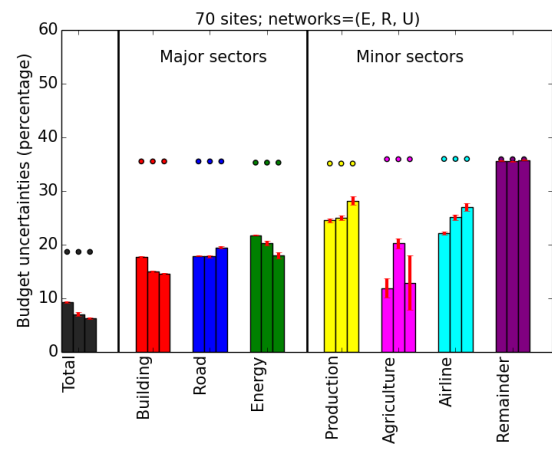
(a)



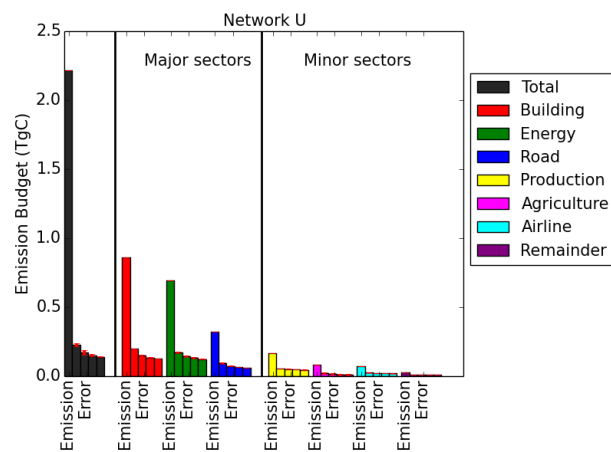
(b)



(c)



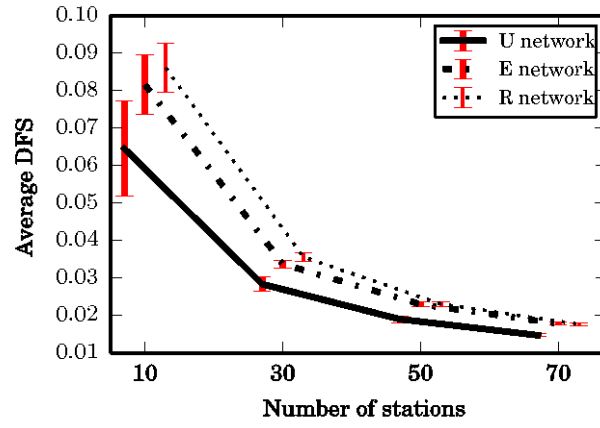
(d)



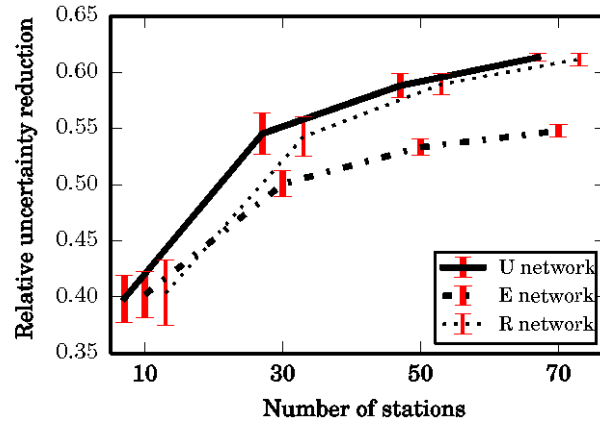
(e)

Fig. 9 Budget of uncertainties in total and sectoral emission estimates by inversions using three types of networks of different sizes. Each sector has a distinct color. In (a-d), we show the uncertainty budgets in percentage to the corresponding emission budgets computed using the IER inventory. The points indicate the percentage of prior uncertainty budgets before inversion, and the bars demonstrate the percentage of posterior uncertainty budgets after inversion. The error bars show the variations of the uncertainty budget using 10 different networks of same size (10, 30, 50, or 70) constructed as detailed in Sect. 2.3. (a-c) Reduction of uncertainties by inversions using three different types of networks of increasing sizes. For each sector, the numbers of stations corresponding to the four bars from left to right are 10, 30, 50 and 70 respectively. (d) Reduction of uncertainties by inversions using three different types of networks of 70 stations. The types of network corresponding to the three bars from left to right are E, R, and U respectively. (e) Comparison between the inventory budgets and uncertainty budgets (both in TgC) using the uniform network of increasing sizes. For each sector, the leftmost bar shows the inventory budget, and the four remaining bars to the right show the budget of uncertainties in posterior emission estimates by inversions using 10, 30, 50 and 70 stations respectively.

1



(a)



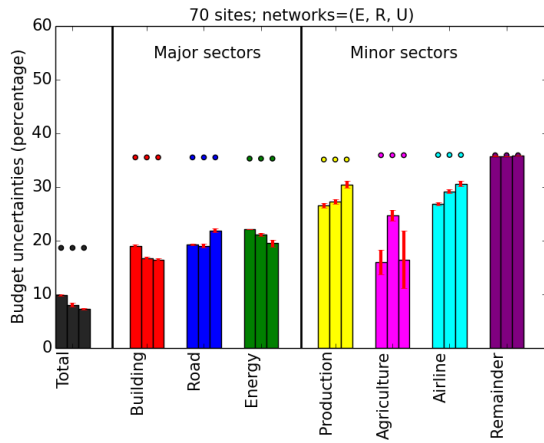
(b)

2

3 Fig. 10 For three types of networks of different sizes, we compute (a) the average DFS which
 4 is total DFS divided by the total number of observations assimilated; and (b) the relative
 5 reduction of uncertainties in scaling factor estimates computed by $(\sqrt{\mathbf{1}^T \mathbf{B} \mathbf{1}} - \sqrt{\mathbf{1}^T \mathbf{A} \mathbf{1}}) /$
 6 $\sqrt{\mathbf{1}^T \mathbf{B} \mathbf{1}}$, where $\mathbf{1}$ is an all-one vector. The error bars show variations due to inversions using
 7 10 different networks of same size constructed as detailed in Sect. 2.3.

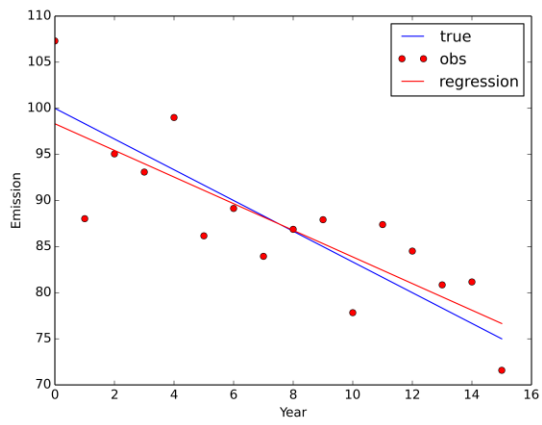
8

1

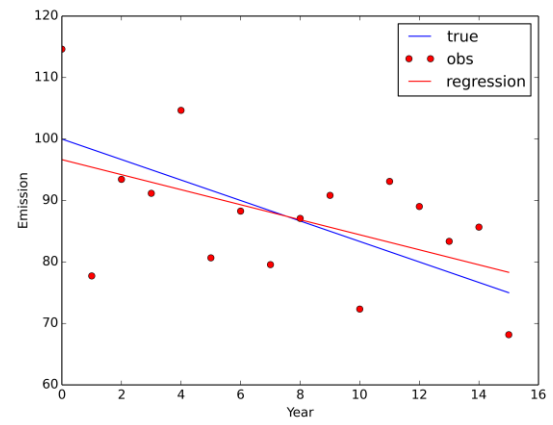


2 Fig. 11 Reduction of uncertainties by inversions using three different types of networks of 70
3 stations with inflated observation error standard derivation (50% larger).

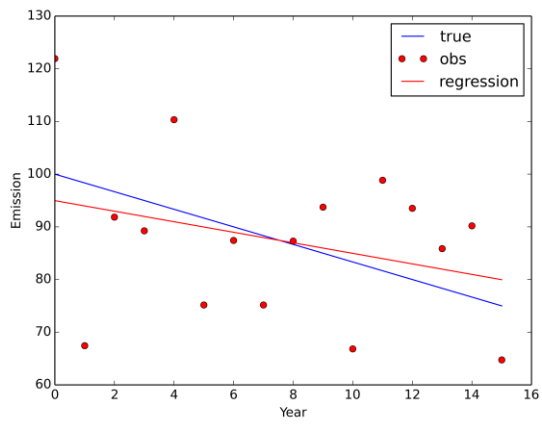
4



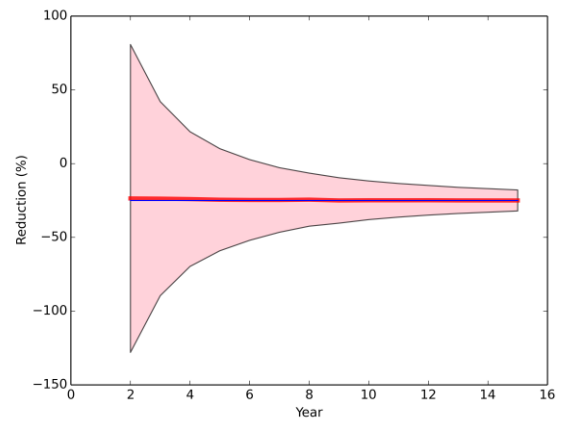
(a)



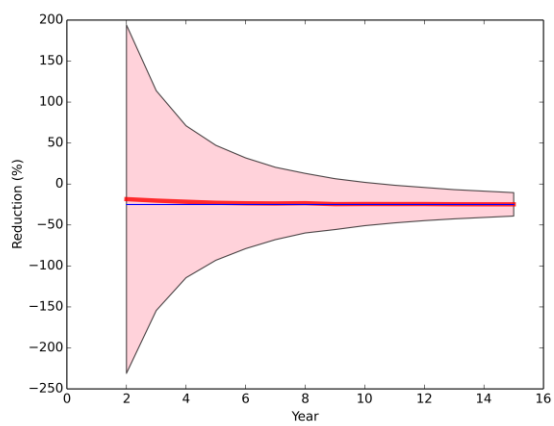
(b)



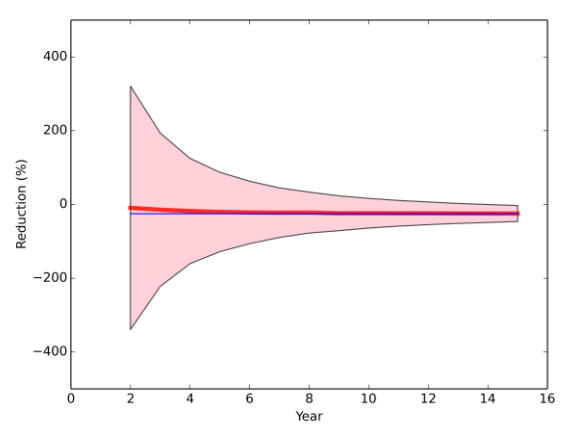
(c)



(d)



(e)



(f)

Fig. C1 Detection of linear trends using the Monte Carlo method with ensembles of 10000 simulations. We hypothesize that the emissions decrease linearly from a value of 100 in any appropriate unit to 75 (i.e. a 25% reduction) in a 15-years time horizon. (a), (b) and (c) show the linear trends detected by linear regressions (red lines) using series of emissions, which are obtained by perturbing the hypothesized emission values (blue lines) under 5%, 10% and 15% 2-sigma annual emission uncertainties respectively (in percentage to the emission value in the initial year). (d), (e) and (f) show the increasing 2-sigma accuracy of the trend detections with increasingly available emission data along years. The detection accuracy is calculated from statistics of regression results for 10000 simulations.